Survey of Existing Algorithms for the Selection of Auxiliary Data MIPAS Special Modes Study WP1400 ESA Contract 16700/02/I-LG

Anu Dudhia
Oxford University, Oxford, UK

August 20, 2003

Abstract

In this report the existing algorithms for the generation of auxiliary data (microwindows, cross-section look-up tables, occupation matrices) for the operational processing of MIPAS L2 data are reviewed.

Using the existing microwindow database, occupation matrices are constructed for the key species (pT, CH_4, H_2O, HNO_3, N_2O, NO_2, O_3) for the nominal mode plus six 'special modes' on the assumption that profiles are retrieved at each tangent point. For the nominal mode this extends the current altitude range of the operational retrievals. For the special modes, it appears that useful accuracy can only be achieved for modes S1, S4 and S5.

Additional species which may be retrieved by MIPAS are considered and the following are suggested for incorporation into an operational retrieval (in order of decreasing accuracy): CFC-12, $ClONO_2$, CFC-11, HCFC-22, NH_3, COF_2 and SF_6.

The retrieval of 3 further species, CO, NO and CO_2, is discussed, but these require modifications to the current operational algorithm.

Contents

1 Microwindow Selection

1.1 Introduction

Several of the current generation of earth-observing satellite instruments are designed to make continuous measurements of atmospheric IR spectra either using grating spectrometers (AIRS[1]) or interferometers (IMG[2], MIPAS[3], IASI[4], TES[5]). Such spectra typically provide thousands of radiance measurements every second, too many to incorporate into a real-time retrieval scheme given present computing speeds. Consequently, attention has been focussed on methods for determining the optimum subsets of such spectra ('microwindows') which contain most of the potential information.

One approach is to simulate the propagation of random noise through the retrieval and select measurements which maximize the information content or degrees of freedom of the signal[6],[7], or which best satisfy other criteria[8]. While this is reasonable if the retrieval errors are predominantly due to random measurement errors and/or errors in the *a priori* estimate, it does not allow for other (systematic) sources of error associated with unretrieved parameters. For example, it does not allow for the uncertainties in modeling the concentrations of the various contaminant species which may also affect a particular spectral region.

An alternative approach[9],[10] addresses this problem by selecting microwindows which minimize the total error, including both random and systematic components. However, this is only achieved by approximating the profile retrieval as a set of independent, single-layer retrievals. As a result, the effect of inter-level correlations in the actual retrieval is ignored. There is also the practical difficulty of consolidating the microwindows derived independently for each profile level into single microwindows applicable over the whole profile.

Microwindows for the operational MIPAS retrieval were selected using a third approach which includes simulating a full profile retrieval including the propagation of systematic error terms[11]. As such, it can be considered either as an extension of the first ('random error') method to include systematic errors, or as a multi-layer version of the second ('single-layer') method.

As well as selecting microwindows, this scheme also allows existing microwindows to be ordered according to different criteria and provides a complete error analysis of the resulting retrieval products.

In the following the MIPAS scheme is outlined and discussed in the context of this study.

1.2 Retrieval Model

A linear approximation can be used to relate the retrieved state vector $\mathbf{x}$ to set of measurements $\mathbf{y}$ via a *Gain Matrix* $\mathbf{G}$ (e.g., [12])

$$\mathbf{x} = \mathbf{G}\mathbf{y} \quad (1)$$

$$\mathbf{G} = \mathbf{S}_a\mathbf{K}^T\left(\mathbf{S}_y + \mathbf{K}\mathbf{S}_a\mathbf{K}^T\right)^{-1} \quad (2)$$

where $\mathbf{S}_a$ is the *a priori* covariance, $\mathbf{S}_y$ is the measurement noise covariance $\mathbf{K}$ is the *Jacobian Matrix*, $K_{ij} = \partial y_i/\partial x_j$. Here it is assumed that spectral selection only depends on vertical domain so that only a one-dimensional retrieval is modelled.

The total error covariance is the sum of the random error plus systematic error terms

$$\mathbf{S}_x^{\text{tot}} = \mathbf{S}_x^{\text{rnd}} + \mathbf{S}_x^{\text{sys}} \quad (3)$$

Two further assumptions are made:

1. Assume that systematic error sources i can be split into independent components $\mathbf{S}_y^i$

$$\mathbf{S}_x^{\text{tot}} = \mathbf{G}\mathbf{S}_y\mathbf{G}^T + \sum_i \mathbf{G}\mathbf{S}_y^i\mathbf{G}^T \quad (4)$$

2. Assume that each independent systematic error component is fully correlated $\mathbf{S}_y^i = (\delta\mathbf{y}^i)(\delta\mathbf{y}^i)^T$

$$\mathbf{S}_x^{\text{tot}} = \mathbf{G}\mathbf{S}_y\mathbf{G}^T + \sum_i \left(\mathbf{G}\delta\mathbf{y}^i\right)\left(\mathbf{G}\delta\mathbf{y}^i\right)^T \quad (5)$$

Thus systematic errors are represented in terms of *Error Spectra* $\delta\mathbf{y}^i$

1.3 Figure of Merit

Some *ad hoc* scalar parameter H is required to define the quality of a retrieval, conveniently expressed in 'bits'

$$H = -\frac{1}{2}\log_2 F \quad (6)$$

where F is some scalar function of the retrieval covariance (smaller $F \Rightarrow$ larger $H \Rightarrow$ better retrieval).

For the specific case where F is the ratio of the determinants of the retrieved/(*a priori*) covariances

$$F = \frac{|\mathbf{S}_x^{\text{tot}}|}{|\mathbf{S}_a|} \quad (7)$$

then H is the *Shannon Information Content.*

However, for MIPAS operational microwindows a different functional form has been used

$$F = \frac{\prod_j \left(S_{x_{jj}}^{\text{tot}} + 2S_{x_{jj}}^{\text{sys}}\right)}{\prod_j S_{a_{jj}}^{\text{tot}}} \quad (8)$$

Compared with the Shannon Information Content,

- Only minimise diagonal elements rather than full matrix
- Additional weight against systematic errors

Evaluating the figure of merit using only the diagonal elements of the covariance matrix is considered to be preferable, especially when considering microwindows for joint-retrievals of two or more species, since the correlation information represented by the off-diagonal elements is often of no practical benefit to users of the data. However, when considering microwindows for species with low S/N, the second feature (weighting against systematic errors) may be dropped.

1.4 Atmospheric Scenarios

It is known (e.g,[13]) that microwindows selected for one particular set of atmospheric conditions may perform poorly in other situations. For example, polar winter conditions are characterised by low temperatures and low contaminant concentrations, suggesting that microwindows with good precision (i.e., S/N) are required, while for other latitudes good accuracy may be a more important criterion.

One solution is to have a set of microwindows selected for different latitudes/seasons, switching between these around the orbit. However, this implies discontinuities in the characteristics of the retrieved profiles whenever a switch occurs. For MIPAS the approach has been to optimise the microwindow selection allowing for a wide range of atmospheres simultaneously.

Mathematically, this is performed by extending the definition of the Figure of Merit (Eq. 6) to be the sum of figures of merit H_i evaluated for N different atmospheres simultaneously

$$H = \sum_{i=1}^{N} a_i H_i \tag{9}$$

where a_i are the weights applied to each atmosphere.

For MIPAS, 5 different atmospheres have been used to represent a 'global' optimisation:

1. Mid-latitude day-time ('day')
2. Mid-latitude night-time ('ngt')
3. Equatorial day-time ('equ')
4. Polar summer (i.e., day-time) ('sum')
5. Polar winter (i.e., night-time) ('win')

and the weights are 1/6 for the first four atmospheres and 1/3 for the polar winter atmosphere, reflecting its additional scientific importance.

1.5 Spectral Masks

Microwindows are defined by boundaries in the wavenumber and tangent altitude domains. The selection algorithm starts with a single point in the domain and then grows microwindows by adding adjacent points either ...

edgewise where every point within the boundaries is used in the retrieval, resulting in *rectangular microwindows*

pointwise where certain points remain excluded, resulting in *masked microwindows.*

The process continues until all any further added points result in a drop in the Figure of Merit or the maximum width (3cm^{-1}, 121 spectral points) is reached.

- Masked microwindows tend to be larger and better optimised for a particular viewing geometry
- Rectangular microwindows tend to be smaller but more generally applicable
- Hybrid option: maintain boundaries but reassign masks for different circumstances.

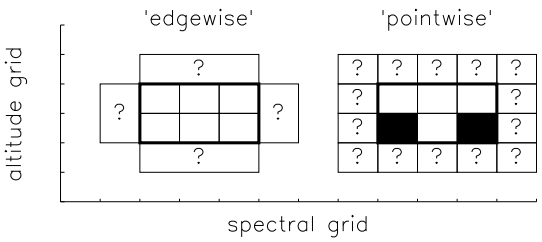

Figure 1: Sketch indicating two possible methods of growing microwindows. A microwindow, currently bounded by the thick line, contains 6 measurements (3 spectral points × 2 tangent altitudes). Growing 'edgewise' all points along one boundary are tested together and, if this improves the Figure of Merit, the microwindow is expanded in that direction. Growing 'pointwise' all points along the boundary are tested individually, and only those points with positive impact on the Figure of Merit are included. This can leave 'masked' points within the microwindow, as indicated by solid squares, corresponding to measurements which are excluded from the retrieval.

1.6 Error Sources/Estimation

In principle, any non-retrieved parameter which contributes significantly either to the forward model or the instrument model uncertainty.

Those used for MIPAS, with revisions based on experience based on in-flight data, are:

Random Due to the propagation of instrument noise through the retrieval. Based on in-flight values of NESR from orbit 2081, allowing for apodisation These replace the pre-launch version based on Flight Model test results, which were for a 'cold' instrument case (205 K) and rather smaller.

NONLTE Non-LTE error. Due to assumption of local thermodynamic equilibrium when modelling emission in the MIPAS forward model. Based on calculations using vibrational temperatures supplied by M.Lopez-Puertas, IAA, Granada, as part of the AMIL2DA project[14]

SPECDB (formerly referred to as HITRAN) Spectroscopic database errors. Due to uncertainties in the strength, position and width of infrared emission lines. Based on estimates supplied for each molecule/band by J.M.Flaud, LPM, Paris.

GAIN Radiometric Gain Uncertainty. Due mostly to non-linearity correction in bands A, AB and B. A uniform value of $\pm 2\%$ has been assumed for all bands (replaces pre-launch value of 1%)

SPREAD (replaces previous ILS error) Uncertainty in width of apodised instrument line shape (AILS). A value of 2% has been assumed based on observed 2nd derivative signatures in the residual spectra during the first 6 months of operation.

SHIFT Uncertainty in the spectral calibration. The design specification of $\pm 0.001 \mathrm{cm}^{-1}$ has been used, and is consistent with the 1st derivatives signatures in the residual spectra.

CO2MIX CO2 line-mixing. Due to neglecting line-mixing effects in the retrieval forward model (only affects strong CO2 Q branches in the MIPAS A and D bands)

CTMERR Uncertainty in gaseous continua. Assumes an uncertainty of $\pm 25\%$ in the modelling of continuum features of H2O (mostly), CO2, O2 and N2.

GRA Horizontal gradient effects. Due to retrieval assuming a horizontally homogeneous atmosphere for each profile. Error is calculated assuming a $\pm$1K/100km horizontal temperature gradient. This could be removed for 2-dimensional retrievals.

HIALT Uncertainty in high-altitude column. Retrieval assumes a fixed-shape of atmospheric profile above the top retrieval level. Effect is calculated assuming 'true' profile can deviate by climatological variability. This has been added since launch.

TEM Temperature propagation error. Temperature and pressure are retrieved first, this represents the contribution of a nominal 1K temperature error into the constituent retrievals. NB: A more accurate assessment of this component is included in the L2 product and is typically 50% larger

PRE Pressure propagation error. As with temperature, effect of a nominal 2% pressure retrieval uncertainty NB: A more accurate assessment of this component is included in the L2 product and is typically 50% larger

species Uncertainties in assumed profiles of contaminant species. For most species this is the climatological 1-sigma variability (profiles supplied by J.Remedios, U.Leicester). However, for contaminant species which are also retrieved by MIPAS (i.e. CH_4, H_2O, HNO_3, N_2O, NO_2, O_3) a smaller uncertainty (say 10%) could be used if it is assumed that the retrieved profiles are usually available.

1.7 Handling Non-LTE Effects

For microwindow selection there are 4 options

1. Assume retrieval forward model has no NLTE modelling. Error spectra $\delta\mathbf{y}$ contain difference between NLTE-LTE calculation (current baseline)

2. Assume retrieval forward model contains inaccurate NLTE modelling (e.g., climatological vibrational temperature profiles). Error spectra $\delta\mathbf{y}$ contains difference between NLTE and perturbed NLTE calculation, perturbation represent 1-σ inaccuracy modelling of NLTE effects (e.g., climatological variability of VT)

3. Assume retrieval forward model contains perfect NLTE modelling (e.g., from external source). NLTE effects do not affect MW selection

4. Assume retrieval forward model retrieves NLTE modelling parameter (e.g., vibrational temperature). Include in state vector $\mathbf{x}$ and calculate Jacobian spectra (e.g., change in radiance due to 1 K change in vibrational temperature)

2 Look Up Tables

2.1 Introduction

The inversion of infra-red satellite measurements to obtain profiles of atmospheric temperature and composition generally starts with an assumed profile. A 'forward model' is then used to calculate the expected measurements from such a profile, these are compared with the observed measurements and the profile adjusted iteratively until convergence is achieved. The forward model is usually the most time consuming part of the retrieval process and, while the precision of the retrieved products may be determined by the instrument noise, the accuracy is often limited by the approximations used in the forward model.

To model a radiance measurement R requires calculations along the following lines (subscript ν denoting spectrally varying quantities and superscript i denoting molecule-dependent quantities):

$$R = \int L_\nu \phi_\nu \, d\nu \tag{10}$$

$$L_\nu = \int B_\nu \frac{d\tau_\nu}{ds} \, ds \tag{11}$$

$$\tau_\nu = \prod_i \tau_\nu^i \tag{12}$$

$$\tau_\nu^i = \exp\left(- \int k_\nu^i \rho^i \, ds \right) \tag{13}$$

where L_ν is the monochromatic radiance at wavenumber ν, ϕ_ν is the channel spectral response, B_ν is the Planck function (local thermodynamic equilibrium assumed), τ_ν the transmittance to the satellite from point s along the ray path, τ_ν^i the transmittance of species i with density ρ^i and k_ν^i the absorption coefficient (we will drop the superscript i from now for simplicity). For limb-sounders, there is usually an additional convolution in the elevation-angle domain to represent the finite field-of-view.

The most accurate method of evaluating the absorption coefficient k_ν is a 'line-by-line' calculation [15] [16] [17] [18]: a summation of the contributions of all spectroscopic lines in the vicinity, each modeled using the appropriate local path conditions of pressure, temperature, and, occasionally, absorber density. However, such calculations are usually too time-consuming to form part of a near real-time retrieval.

To model satellite measurements in near real time, the usual approach is to use a band model [19] [20] [21] [22]. For these, the order of the spectral and path integrations in Eqs. 10 and 11 is reversed, so that the monochromatic transmittance can be replaced by a spectrally averaged value $\bar{\tau}$, either computed for the entire channel response or smaller intervals. These band-transmittances are pre-computed for a variety of path conditions, leaving just the path integration in the forward model. While this is extremely fast, band transmittances do not follow Beer's Law (Eq. 13) so further assumptions have to be made when obtaining the transmittance increments $d\bar{\tau}/ds$ and handling multiple absorbers ($\bar{\tau} \neq \prod_i \bar{\tau}_i$), and this fundamentally limits the accuracy of this approach.

Given current computing speeds, a reasonable compromise might be to use the monochromatic radiative transfer (Eqs. 10–12) but, rather than evaluate k_ν using a line-by-line model, use look-up tables containing values which have been pre-computed for a range of path conditions (e.g., [23]). The main drawback to this direct tabulation approach is that, in order not to introduce significant interpolation errors, the absorption coefficient tables tend to be rather large and if these cannot be contained within the computer memory significant time can spent accessing the data from disk. Various techniques for compressing the look-up tables have been suggested, such as parameterizing the temperature dependence by a polynomial, or using singular value decomposition (SVD) [24]. These require additional CPU time in order to reconstruct the absorption coefficients, but this may be outweighed by the benefits of reducing the data to a size which can be contained within the computer memory.

So far, such techniques had only been considered for nadir-viewing instruments, but were adapted for the operational processing of MIPAS. The MIPAS L2 retrieval[25] has a monochromatic forward model which uses SVD-compressed look-up tables ('LUTs') of absorption coefficients and is further optimized by using quadrature points ('irregular grids') for the spectral integration. The generation of these data has been described in [26].

2.2 CPU Considerations

MIPAS acquires spectra covering 685–2410 cm^{-1} at 0.025 cm^{-1} spacing every 4.6 s. A typical limb scan sequence from 68–6 km comprises 17 such spectra and from these data profiles of temperature and six species are retrieved (although not for all tangent altitudes). Only small subsets ('microwindows') of the spectra will be used in the retrievals[10][11], totalling around 10 cm^{-1} per spectrum per retrieved species. With 40 measurements/cm^{-1}, this means that the near real time processing absorbs ~500 measurements every second.

The spectral integration (Eq. 10) behaves monochromatically if it is performed at a sufficiently fine spacing to resolve atmospheric lines. A resolution of 0.0005 cm^{-1} is usually considered adequate (since Doppler broadening limits lines to a minimum half-width of around 0.001 cm^{-1}), giving 50 radiance calculations for each MIPAS measurement on a 0.025 cm^{-1} grid. By simultaneously modeling multiple tangent paths for the entire limb-scan, a

high degree of replication is possible so that each additional spectrum, including FOV convolution, only requires about 10 additional calculations of k_ν for the whole atmospheric path. So to compute transmittances for one gas for one MIPAS measurement requires about $50 \times 10 = 500$ computations of k_ν. Allowing for 10 absorbing species per microwindow and four retrieval iterations this gives a figure of 10^7 k_ν computations every second.

To compute the absorption coefficient with a line-by-line model using some version of the Humlíček algorithm[27] requires 10–100 floating-point operations (FLOPs) per line so, considering 10–100 local lines, typically 10^3 FLOPs per absorption coefficient. Thus, to retrieve MIPAS data in near real time using a line-by-line forward model would require a 10 Giga-FLOP processor. By using look-up tables, where the absorption coefficients can be obtained in <100 operations, this is reduced to <1 Giga-FLOPs. In practice, the radiative transfer calculations become the limiting term rather than the k_ν computation, but both can be further reduced by a factor 3–10 if the integration is performed explicitly on a subset of quadrature points from the 0.0005 cm^{-1} grid.

2.3 Accuracy Criteria

The representation of absorption coefficient by means of look-up tables is a three-way compromise between storage space, CPU time and accuracy, so some accuracy requirement also has to be specified.

It is simple to express the accuracy in terms of the difference between the interpolated absorption coefficient and a 'true' value calculated with a line-by-line method. However, it is the accuracy of the forward model calculation that is of interest, and this can only be determined by comparing radiative transfer calculations using both a line-by-line model and look-up tables. For this work, the RFM[18] was used since this could use both line-by-line and LUT calculations of absorption coefficients while keeping all other aspects of the forward calculation the same.

For MIPAS, the requirement is that these forward model calculations should agree to better than 10% of the Noise Equivalent Spectral Radiance (NESR), i.e., that any errors due to the absorption coefficient representation are at least a factor 10 smaller than the expected random noise on each measurement. When viewing a 230 K black body, MIPAS signal/noise values vary from 150–50 in the spectral ranges used for retrievals, so the NESR/10 criterion corresponds to around 0.1% accuracy for an opaque path. While the NESR/10 value may appear conservative, it should be noted that the noise contribution to retrieval error is random and therefore reduced by adding more measurements or averaging profiles, but the forward model errors may be systematic and their contribution remains constant.

The forward model error limit is not necessarily the best criterion that could be used. A relatively straightforward modification would be to use a single-layer Jacobian analysis[9] to convert this into retrieval error, which would then weight the error of each measurement according to its impact on the retrieval. However, the simpler criterion has chosen mainly on the grounds that it does not distort the residual spectra from the retrievals.

2.4 Procedure

It is assumed that k_ν can be tabulated as a function of wavenumber ν, pressure p and temperature T only, ignoring any dependence on absorber density. Self-broadening of water vapor lines can be significant in the lower troposphere, but clouds usually prevent infrared limb sounders from viewing these altitudes.

The first step is to use a line-by-line model to create (large) look-up tables (LUTs) each representing $k(\nu, p, T)$ for one absorbing species in one microwindow. The wavenumber axis has a spacing 0.0005 cm^{-1} and extends ± 0.175 cm^{-1} beyond the nominal microwindow boundaries to allow for convolution with the apodised instrument line shape (AILS). The temperature axis spans 180–310 K, the extreme range of atmospheric temperatures expected, while the pressure axis depends on the range of tangent altitudes for which the microwindow is defined. For the major absorbers within each microwindow, a total of 2500 (p, T) points are calculated, with typically 12 points for every factor 10 along the pressure axis and 2 K increments along the temperature axis.

The optimization consists of three stages:

1. Subsample the p, T axes
2. Compress the table using SVD
3. Subsample the wavenumber axis

At each stage the calculations are compared with reference line-by-line calculations for a typical atmosphere and both maximum and minimum extreme profiles of the target species.

In stage 1 the original high-resolution p, T axes are subsampled with increasing integer intervals (i.e., reduced by factor 2, 3, 4, etc) until a maximum discrepancy of NESR/30 is reached.

In stage 2 the reduced tables from stage 1 are compressed using singular value decomposition (see section 2.5) to a large number (30) of singular values. The tables are then reconstructed using progressively fewer singular values until the maximum discrepancy reaches NESR/15.

In stage 3 the SVD-compressed tables from stage 2 are used to calculate spectra at 0.0005 cm^{-1} resolution and convolved with the AILS. Spectral points are

then progressively removed from this 'full' fine-grid and replaced by interpolated values in the convolution the maximum discrepancy reaches NESR/10.

2.5 Singular Value Decomposition

Any matrix $\mathbf{K}$ $(m \times n)$ can be decomposed as the product of three other matrices:

$$\mathbf{K} = \mathbf{U}\mathbf{\Sigma}\mathbf{V} \tag{14}$$

where $\mathbf{U}$ $(m \times n)$ and $\mathbf{V}$ $(n \times n)$ are orthonormal matrices, and $\mathbf{\Sigma}$ is a diagonal matrix containing n singular values ([28], for example, contains further details). Assuming that most of the information is contained in the l $(\ll n)$ largest singular values, the decomposition matrices can be truncated in the n dimension to give:

$$\mathbf{K} \simeq \mathbf{U}'\mathbf{\Sigma}'\mathbf{V}' = \mathbf{U}'\mathbf{W}' \tag{15}$$

where the reduced matrices $\mathbf{U}'$ $(m \times l)$ and $\mathbf{W}'$ $(l \times n)$ are much smaller matrices than the original matrix $\mathbf{K}$, giving a compression factor l/n (assuming $m \gg n$).

In this application, the matrix $\mathbf{K}$ represents $\ln k$ tabulated for m wavenumber points and n (p, T) combinations. The compression factor l/n is therefore given by the ratio of the number of singular values to the number of (p, T) points.

3 Special Mode OMs

3.1 Introduction

This section deals with the selection of microwindow occupation matrices to retrieve the key species (pT, CH_4, H_2O, HNO_3, N_2O, NO_2, O_3) for the various 'Special Observation' modes. For comparison, microwindows used in the current operational processing for the nominal mode observations are listed in Table 1.

For these selections only microwindows in the existing database have been used, including those generated previously for 0.1 cm^{-1} resolution (numbered #60–79). For each special mode, it is assumed that all spectra are flagged as 'valid' so that just a single occupation matrix has been generated for each species.

Selection is mostly influenced by the set of tangent altitudes for each special mode: here it is assumed that that the retrieved profiles are on the same set of tangent altitudes. To a lesser degree, the selection is affected by the atmospheric scenario(s) chosen for the optimisation (section 1.4).

The microwindows selected for operational use in the nominal mode have been selected attempting to limit CPU requirements as well as minimising the total error. However, for the special modes, the only criterion used here is minimising the total error.

The plots show the expected accuracy profiles for the retrieved species in different colours/symbols. Solid lines/symbols represent accuracy, dotted lines and open symbols precision. The top axis is for temperature and pressure, the bottom axis for volume mixing ratio. The horizontal lines represent the tangent altitudes for each mode. The dashed vertical line at 3K, 3% pressure or 30% VMR is an arbitrary definition of 'useful' accuracy. In the key to the plots, the figure in brackets lists the number of microwindows used for each species, details of which are given in the tables.

Table 1: Microwindows selected for the current nominal occupation matrix.

MW Label	Waveno. Range		Alt.		NPts
PT_0001	686.400	689.400	30	68	1089
PT_0004	728.300	729.125	15	27	170
PT_0037	694.800	695.100	27	36	52
PT_0038	700.475	701.000	21	30	88
PT_0039	685.700	685.825	33	47	30
PT_0002	791.375	792.875	12	33	488
PT_0006	741.975	742.250	15	24	48
				Total:	1965
CH4_0012	1227.175	1230.175	12	60	1694
CH4_0001	1350.875	1353.875	12	60	1694
				Total:	3388
H2O_0001	1650.025	1653.025	15	60	1573
H2O_0002	807.850	808.450	12	18	75
H2O_0007	1645.525	1646.200	27	60	252
				Total:	1900
HNO30006	885.100	888.100	12	42	1331
HNO30001	876.375	879.375	12	42	1331
				Total:	2662
N2O_0001	1272.050	1275.050	12	47	1452
N2O_0004	1256.675	1257.975	12	30	371
				Total:	1823
NO2_0001	1607.275	1610.275	24	47	968
NO2_0003	1613.725	1616.600	24	47	928
NO2_0013	1622.550	1623.475	24	30	114
				Total:	2010
O3_0021	763.375	766.375	12	60	1694
O3_0013	1039.375	1040.325	52	60	78
O3_0001	1122.800	1125.800	12	60	1694
				Total:	3466
				Grand Total:	17214

3.2 Extended Range Nominal Mode

The nominal mode consists of 17 sweeps at tangent heights 68, 60, 52, 47, 42 ... 6km in 3km steps. Currently the retrievals are limited to a lower altitude of 12 km and an upper altitude determined by an achievable accuracy of 25% or better. The microwindows used are listed in Table 1.

If the retrieval range is extended down to 6 km (in the absence of clouds) and exploiting higher altitudes where possible while still requiring the CPU limitation, new occupation matrices can be constructed as shown in Table 2. Note that the microwindows are substantially the same, just used over an extended altitude range. Fig. 2 shows the expected accuracy profiles for the key species for this case.

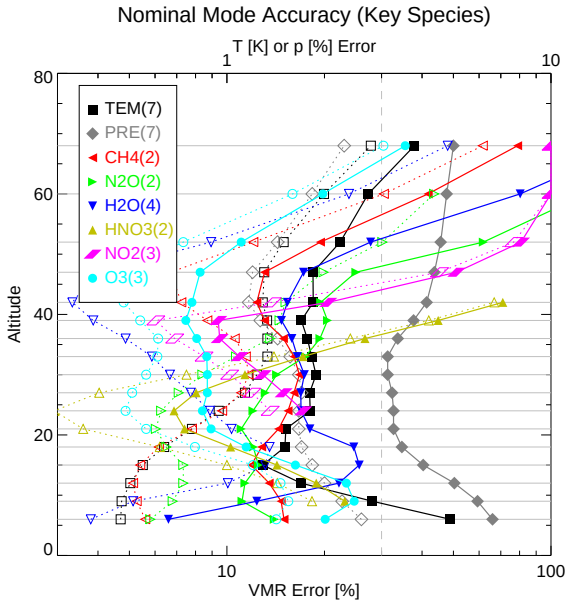

Figure 2: Accuracy profiles for the key species retrieved in a mid-latitude day-time atmosphere using the 'extended range' nominal mode occupation matrix.

Table 2: Microwindows selected for the nominal mode for extended-range retrievals 6–68 km.

MW Label	Waveno. Range		Alt.		NPts
PT_0001	686.400	689.400	30	68	1089
PT_0004	728.300	729.125	15	27	170
PT_0037	694.800	695.100	27	36	52
PT_0038	700.475	701.000	21	30	88
PT_0039	685.700	685.825	33	47	30
PT_0002	791.375	792.875	6	33	610
PT_0006	741.975	742.250	15	24	48
				Total:	2087
CH4_0012	1227.175	1230.175	6	60	1936
CH4_0001	1350.875	1353.875	12	68	1815
				Total:	3751
H2O_0001	1650.025	1653.025	15	68	1694
H2O_0022	946.650	947.700	6	18	215
H2O_0002	807.850	808.450	9	18	100
H2O_0007	1645.525	1646.200	27	60	252
				Total:	2261
HNO30006	885.100	888.100	9	42	1452
HNO30001	876.375	879.375	9	42	1452
				Total:	2904
N2O_0001	1272.050	1275.050	12	60	1694
N2O_0012	1233.275	1236.275	6	27	968
				Total:	2662
NO2_0001	1607.275	1610.275	24	68	1331
NO2_0003	1613.725	1616.600	24	68	1276
NO2_0013	1622.550	1623.475	24	30	114
				Total:	2721
O3_0021	763.375	766.375	6	68	2057
O3_0013	1039.375	1040.325	52	68	117
O3_0001	1122.800	1125.800	6	68	2057
				Total:	4231
				Grand Total:	20617

3.3 S1: Polar Chemistry

Special mode S1 is intended to investigate polar chemistry and dynamics. It uses 14 sweeps at altitudes 55, 45, 35, 30, 27 ... 13km in 2km steps, 10, 7km. However there is a latitude-dependent offset varying from +2km at the equator to −2km at the poles centred on 8km. Since the main purpose is for polar studies, the occupation matrix is selected by optimising for a polar-winter atmosphere on the 55 ... 7km tangent altitudes. The accuracy profiles for the key species are shown in Fig. 3 and the selected microwindows listed in Table 3.

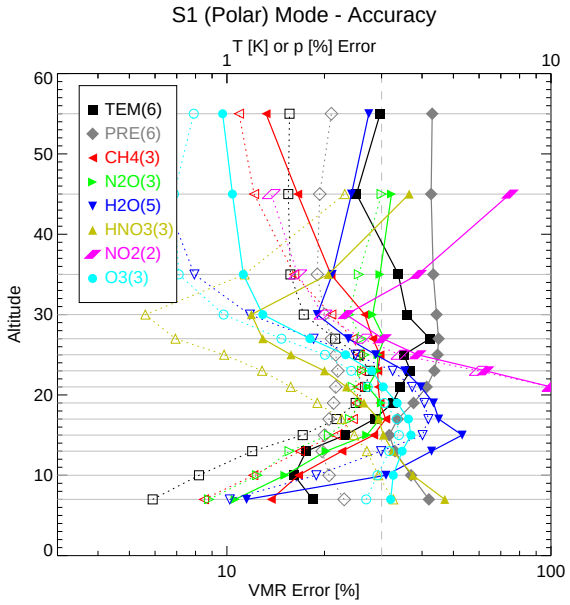

Figure 3: Accuracy profiles for the key species retrieved in a polar winter atmosphere using the S1 special mode occupation matrix.

Table 3: Microwindows selected for the S1 special mode occupation matrix

MW Label	Waveno. Range		Alt.		NPts
PT_0002	791.375	792.875	7	30	671
PT_0001	686.400	689.400	30	55	484
PT_0006	741.975	742.250	15	23	60
PT_0038	700.475	701.000	21	30	110
PT_0021	1932.850	1934.350	13	55	732
PT_0017	696.200	698.375	27	55	440
				Total:	2497
CH4_0012	1227.175	1230.175	7	55	1694
CH4_0001	1350.875	1353.875	13	55	1452
CH4_0013	1247.775	1248.650	7	30	396
				Total:	3542
H2O_0001	1650.025	1653.025	15	55	1331
H2O_0022	946.650	947.700	7	17	215
H2O_0002	807.850	808.450	10	17	100
H2O_0021	1454.525	1457.525	15	55	1331
H2O_0027	1374.125	1375.075	13	23	234
				Total:	3211
HNO30001	876.375	879.375	7	45	1573
HNO30006	885.100	888.100	7	35	1452
HNO30021	1319.050	1322.050	13	45	1331
				Total:	4356
N2O_0001	1272.050	1275.050	13	45	1331
N2O_0012	1233.275	1236.275	7	27	1210
N2O_0004	1256.675	1257.975	10	30	530
				Total:	3071
NO2_0003	1613.725	1616.600	21	45	812
NO2_0001	1607.275	1610.275	21	45	847
				Total:	1659
O3_0021	763.375	766.375	7	55	1694
O3_0001	1122.800	1125.800	7	55	1694
O3_0012	1073.800	1076.800	10	55	1573
				Total:	4961
				Grand Total:	23297

3.4 S2: Strat/Trop Exchange

Special mode S2 is intended to investigate stratosphere/troposphere exchange processes and tropospheric chemistry. It uses 14 sweeps at altitudes 40, 30, 25, 20 ...5km in 1.5km steps. The occupation matrix is selected by optimising jointly for mid-latitude and equatorial day-time atmospheres. The accuracy profiles for the key species are shown in Fig. 4 and the selected microwindows listed in Table 4.

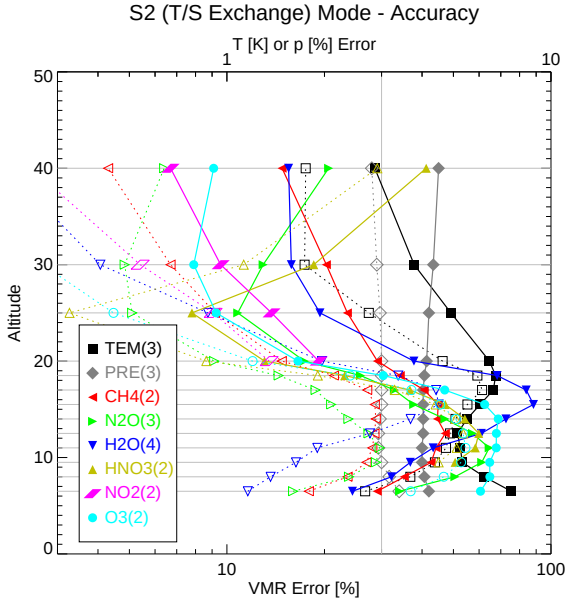

Figure 4: Accuracy profiles for the key species retrieved in a mid-latitude day-time atmosphere using the S2 special mode occupation matrix.

Table 4: Microwindows selected for the S2 special mode occupation matrix

MW Label	Waveno. Range		Alt.		NPts
PT_0035	944.200	946.500	7	17	744
PT_0001	686.400	689.400	30	40	242
PT_0022	1353.325	1354.825	13	40	549
				Total:	1535
CH4_0012	1227.175	1230.175	7	40	1573
CH4_0023	1138.875	1140.075	7	14	294
				Total:	1867
H2O_0022	946.650	947.700	7	17	344
H2O_0007	1645.525	1646.200	30	40	56
H2O_0002	807.850	808.450	10	17	150
H2O_0001	1650.025	1653.025	16	40	847
				Total:	1397
HNO30006	885.100	888.100	10	40	1331
HNO30001	876.375	879.375	10	40	1331
				Total:	2662
N2O_0021	1161.625	1164.625	7	40	1573
N2O_0012	1233.275	1236.275	7	25	1331
N2O_0001	1272.050	1275.050	13	40	1089
				Total:	3993
NO2_0003	1613.725	1616.600	20	40	464
NO2_0001	1607.275	1610.275	20	40	484
				Total:	948
O3_0001	1122.800	1125.800	7	40	1573
O3_0021	763.375	766.375	7	40	1573
				Total:	3146
				Grand Total:	15548

3.5 S3: Aircraft Emissions

Special mode S3 is intended to investigate the impact of aircraft emissions. It uses 11 sweeps at altitudes 40, 30, 23, 18, 15 ...6km in 1.5 km steps. The mode will probably use the side-viewing option, (although this does not affect the occupation matrix selection), viewing north of 25deg latitude. The selection is optimised for the mid-latitude day-time atmosphere. The accuracy profiles for the key species are shown in Fig. 5 and the selected microwindows listed in Table 5.

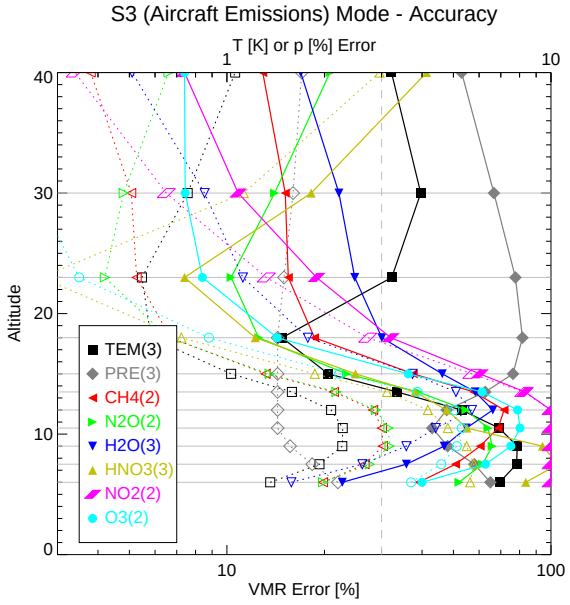

Figure 5: Accuracy profiles for the key species retrieved in a mid-latitude day-time atmosphere using the S3 special mode occupation matrix.

Table 5: Microwindows selected for the S3 special mode occupation matrix

MW Label	Waveno. Range		Alt.		NPts
PT_0002	791.375	792.875	6	30	610
PT_0001	686.400	689.400	30	40	242
PT_0035	944.200	946.500	6	18	744
				Total:	1596
CH4_0012	1227.175	1230.175	6	40	1331
CH4_0001	1350.875	1353.875	12	40	847
				Total:	2178
H2O_0021	1454.525	1457.525	15	40	605
H2O_0028	959.400	959.900	6	15	147
H2O_0027	1374.125	1375.075	12	23	195
				Total:	947
HNO30001	876.375	879.375	6	40	1331
HNO30023	1311.425	1312.350	12	30	228
HNO30006	885.100	888.100	6	40	1331
				Total:	2890
N2O_0001	1272.050	1275.050	12	40	847
N2O_0012	1233.275	1236.275	6	23	1089
				Total:	1936
NO2_0003	1613.725	1616.600	15	40	580
NO2_0010	1619.125	1622.125	15	40	605
				Total:	1185
O3_0001	1122.800	1125.800	6	40	1331
O3_0021	763.375	766.375	6	40	1331
				Total:	2662
				Grand Total:	13394

3.6 S4: Stratospheric Dynamics

Special mode S4 is intended to investigate stratospheric dynamics, transport processes (medium scale structures, ozone laminae ...). It uses 15 sweeps at altitudes 53, 47 ... 8km in 3km steps, scanning in azimuth to produce 3 parallel profile tracks (although this does not affect the microwindow selection). The spectral resolution is reduced by a factor 4 so microwindows are selected from the 0.1 cm^{-1} database. The selection is optimised for 'global' retrievals, i.e., simultaneously for all 5 atmospheric scenarios.

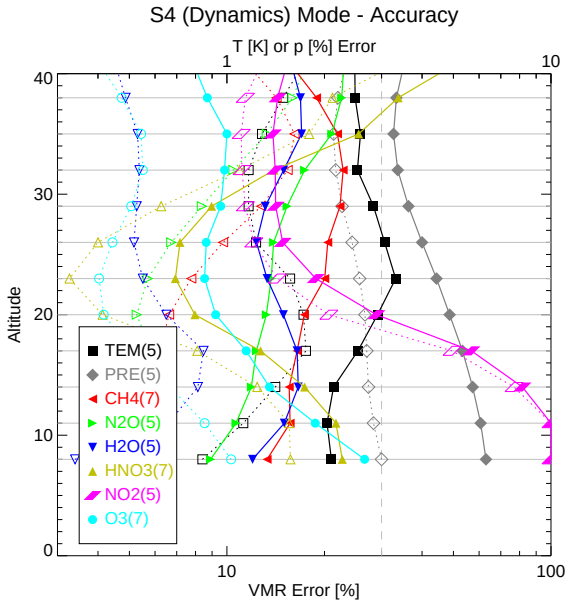

Figure 6: Accuracy profiles for the key species retrieved in a mid-latitude day-time atmosphere using the S4 special mode occupation matrix.

Table 6: Microwindows selected for the S4 special mode occupation matrix

MW Label	Waveno. Range		Alt.		NPts
PT_0070	705.300	708.300	23	53	310
PT_0073	941.300	944.300	8	29	248
PT_0067	754.100	755.100	8	11	22
PT_0063	688.000	688.500	29	41	30
PT_0072	1237.700	1238.300	8	14	21
			Total:		631
CH4_0072	1234.800	1237.800	8	53	465
CH4_0061	1353.900	1356.900	11	53	434
CH4_0070	1371.900	1374.900	14	53	403
CH4_0060	1350.800	1353.800	44	53	93
CH4_0062	1227.200	1230.100	8	11	60
CH4_0073	1244.400	1247.300	11	17	90
CH4_0067	1346.700	1349.600	14	26	150
			Total:		1695
H2O_0070	1652.900	1655.900	17	53	372
H2O_0061	807.500	809.800	8	23	144
H2O_0060	1649.800	1652.800	17	53	372
H2O_0077	1433.700	1436.700	14	53	403
H2O_0068	1454.400	1457.400	17	53	372
			Total:		1663
HNO30060	878.400	881.400	8	53	465
HNO30070	864.000	867.000	8	53	465
HNO30062	894.500	897.500	8	38	341
HNO30068	890.500	893.500	8	53	465
HNO30067	1324.100	1326.900	38	53	145
HNO30061	884.300	887.300	8	41	372
HNO30066	874.900	877.900	8	53	465
			Total:		2718
N2O_0071	1261.900	1264.900	11	53	434
N2O_0061	1160.800	1163.500	8	20	140
N2O_0060	1272.500	1275.500	17	53	372
N2O_0062	1165.100	1168.100	8	14	93
N2O_0075	1265.000	1267.200	14	23	92
			Total:		1131
NO2_0060	1608.500	1611.500	17	53	372
NO2_0070	1611.600	1613.500	23	53	200
NO2_0063	1613.600	1616.600	17	35	217
NO2_0061	1626.700	1629.700	17	32	186
NO2_0075	1596.200	1597.800	44	53	51
			Total:		1026
O3_0060	1073.400	1076.400	8	53	465
O3_0066	1121.300	1124.300	8	38	341
O3_0068	1142.400	1145.400	8	53	465
O3_0070	1068.700	1071.700	8	53	465
O3_0067	1112.300	1115.300	11	47	403
O3_0069	791.200	793.100	8	47	280
O3_0062	806.400	809.400	11	38	310
			Total:		2729
			Grand Total:		11593

3.7 S5: Diurnal Changes

Special mode S5 is intended to investigate diurnal changes. It uses 16 sweeps at altitudes 60 ...15km in 3 km steps, using sideways viewing although this does not affect the microwindow selection. The selection is optimised for the mid-latitude night-time atmosphere.

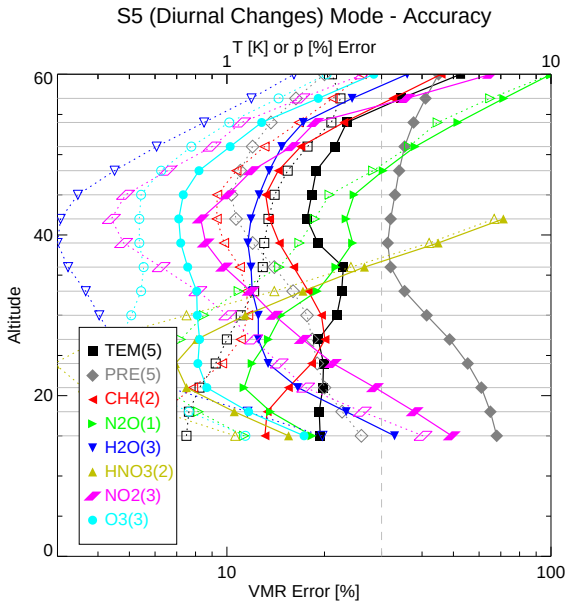

Figure 7: Accuracy profiles for the key species retrieved in a mid-latitude day-time atmosphere using the S5 special mode occupation matrix.

Table 7: Microwindows selected for the S5 special mode occupation matrix

MW Label	Waveno. Range		Alt.		NPts
PT_0001	686.400	689.400	30	60	1331
PT_0004	728.300	729.125	15	27	170
PT_0017	696.200	698.375	27	60	1056
PT_0002	791.375	792.875	15	33	427
PT_0021	1932.850	1934.350	15	60	976
				Total:	3960
CH4_0001	1350.875	1353.875	15	60	1936
CH4_0012	1227.175	1230.175	15	60	1936
				Total:	3872
H2O_0011	1574.800	1577.800	15	60	1936
H2O_0001	1650.025	1653.025	15	60	1936
H2O_0021	1454.525	1457.525	15	60	1936
				Total:	5808
HNO30006	885.100	888.100	15	42	1210
HNO30001	876.375	879.375	15	42	1210
				Total:	2420
N2O_0001	1272.050	1275.050	15	60	1936
				Total:	1936
NO2_0003	1613.725	1616.600	15	60	1856
NO2_0001	1607.275	1610.275	15	60	1936
NO2_0010	1619.125	1622.125	15	60	1936
				Total:	5728
O3_0001	1122.800	1125.800	15	60	1936
O3_0021	763.375	766.375	15	60	1936
O3_0012	1073.800	1076.800	15	60	1936
				Total:	5808
				Grand Total:	29532

3.8 S6: UTLS

Special mode S6 is intended to investigate the upper troposphere/lower stratosphere region. It uses 12 sweeps at altitudes 35, 28, 24 ...6km in 2 km steps. The spectral resolution is reduced by a factor 4 so microwindows are selected from the 0.1 cm^{-1} database. The selection is optimised for 'global' retrievals, i.e., simultaneously for all 5 atmospheric scenarios.

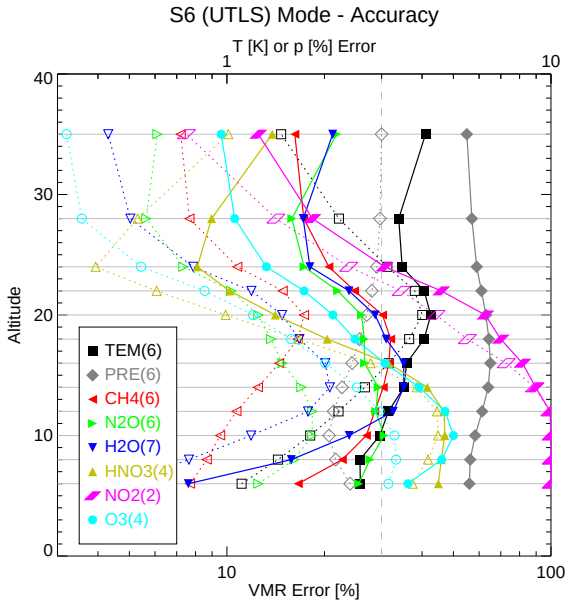

Figure 8: Accuracy profiles for the key species retrieved in a mid-latitude day-time atmosphere using the S6 special mode occupation matrix.

3.9 Summary

Whether or not a useful retrieval can be obtained using the current microwindow database is largely determined by the vertical spacing of the retrieval. If the retrieval follows the measurement tangent heights, as assumed, then 2 km appears to be the minimum spacing for full spectral resolution, and 3 km for 0.1 cm^{-1} resolution.

Consequently, it appears that special modes S1, S4 and S5 may produce useful results using existing microwindows while modes S2, S3 and S6 would not.

Table 8: Microwindows selected for the S6 special mode occupation matrix

MW Label	Waveno. Range		Alt.		NPts
PT_0073	941.300	944.300	6	28	341
PT_0063	688.000	688.500	28	35	12
PT_0072	1237.700	1238.300	6	14	35
PT_0061	685.900	687.800	35	35	20
PT_0076	814.600	816.300	6	20	144
PT_0062	688.600	691.600	28	35	62
				Total:	614
CH4_0061	1353.900	1356.900	10	35	310
CH4_0062	1227.200	1230.100	6	12	120
CH4_0073	1244.400	1247.300	10	18	150
CH4_0072	1234.800	1237.800	6	35	372
CH4_0070	1371.900	1374.900	12	35	279
CH4_0065	1362.300	1365.300	12	35	279
				Total:	1510
H2O_0068	1454.400	1457.400	16	35	217
H2O_0062	955.000	957.300	6	20	192
H2O_0078	1422.900	1425.900	12	24	217
H2O_0077	1433.700	1436.700	12	35	279
H2O_0060	1649.800	1652.800	16	35	217
H2O_0063	945.700	947.100	6	18	105
H2O_0067	838.600	841.600	6	20	248
				Total:	1475
HNO30070	864.000	867.000	6	35	372
HNO30062	894.500	897.500	6	35	372
HNO30075	905.700	908.700	12	35	279
HNO30060	878.400	881.400	6	35	372
				Total:	1395
N2O_0071	1261.900	1264.900	10	35	310
N2O_0061	1160.800	1163.500	6	20	224
N2O_0070	1877.900	1880.900	10	35	310
N2O_0060	1272.500	1275.500	16	35	217
N2O_0069	1243.800	1246.800	16	20	93
N2O_0067	1163.600	1165.000	6	18	105
				Total:	1259
NO2_0063	1613.600	1616.600	16	35	217
NO2_0074	1642.900	1645.800	16	24	150
				Total:	367
O3_0066	1121.300	1124.300	6	35	372
O3_0068	1142.400	1145.400	6	35	372
O3_0067	1112.300	1115.300	10	35	310
O3_0062	806.400	809.400	10	35	310
				Total:	1364
				Grand Total:	7984

4 Additional Species

4.1 Procedure

The general procedure for determining whether a species can be retrieved using the 'standard' retrieval algorithm is as follows:

1. Define profile of species
2. Create Jacobian spectra
3. Select microwindows until some limit is reached
4. Determine retrieval error

In this case the microwindow selection was terminated either when 10 microwindows had been found or a total of 10000 measurements had been used.

For each species, microwindows have only been selected for one of the five standard atmospheres (section 1.4). By default this is the mid-latitude day-time atmosphere, but others have been used where the enhancement for a particular species is significant.

4.2 Summary of Results

Table 9 summarises the results for the additional species investigated. The retrieval altitude range is that for which the accuracy is better than 30%. Information content is defined in two ways. 'Info 1' is the information content relative to a uniform 100% *a priori* uncertainty for all species, and represents the relative accuracy with which these species may be retrieved from MIPAS. 'Info 2' represents the information content relative to the *climatological* uncertainty in these species (considering only levels where the retrieval is more accurate than the climatology). This represents the extent to which MIPAS measurements may improve on current knowledge.

4.3 Occupation Matrices

The current operational processor is limited, by CPU, to handling two or three microwindows, totalling 2000–3000 measurements, per species. With this restriction, occupation matrices have been selected for each of the species listed in Table 9 and seven species appear still to give useful accuracy, as shown in Fig. 9 and listed, in order of viability in Table 10.

These are the gases recommended for consideration if the MIPAS operational processor is extended to include additional target species.

Compared to Table 9, CFC-14 is removed since the retrieval information is spread over a wide altitude range (due to the near constant mixing ratio of this long-lived tracer — section 4.4.2) and 'useful' accuracy can only be achieved with a relatively large number of microwindows. SF_6 is promoted above other molecules since most of the information comes from a single spectral feature (section 4.4.10) and thus much of the overall accuracy is achieved with relatively few microwindows.

Table 9: Information content (in 'bits') for microwindows selected for additional species up to a limit of 10 microwindows (N.MW) or 10^5 measurements (N.Meas). Unless indicated otherwise, selection is for Mid-Latitude daytime conditions.

Species	N.MW	N.Meas	Alt.	Info 1	Info 2
CFC-12	6	$> 10^5$	6–30	31.4	8.6
CFC-14	7	$> 10^5$	12–52	26.5	0
ClONO2$^{(n)}$	7	$> 10^5$	18–39	21.0	11.6
CFC-11	7	$> 10^5$	6–21	20.4	0.4
CFC-22	7	$> 10^5$	6–24	20.4	0.3
NH3	8	$> 10^5$	6–21	18.3	28.3
COF2	10	7821	15–33	16.1	9.4
HCN	10	4153	12–18	15.0	6.5
OCS	10	9604	9–24	14.4	12.2
SF6*	6	7268	6–21	14.1	0
N2O5$^{(n)}$	6	$> 10^5$	15–33	10.2	2.9
C2H6	10	7947	6–15	12.0	3.3
HOCl$^{(p)}$	6	$> 10^5$	18–30	11.6	1.8
SO2	10	7045	12–18	8.2	8.4
H2O2	10	7502	6–9	7.9	3.1
ClO$^{(p)}$	9	$> 10^5$	18–21	5.0	0
CCl4	10	$> 10^5$	9	3.4	0

$^{(n)}$Mid-Lat Nighttime, $^{(p)}$Polar Winter conditions
*SF6: no more microwindows could be found

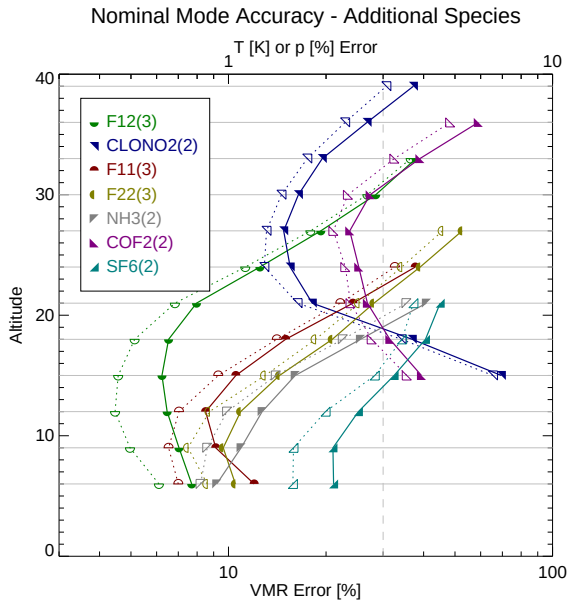

Figure 9: Accuracy profiles for the key species retrieved with the nominal occupation matrix for a mid-latitude day-time atmosphere.

Table 10: Microwindows selected for the nominal occupation matrix for extended-range 6–68 km retrievals.

MW Label	Waveno. Range		Alt.		NPts
F12_0101	921.400	924.400	6	33	1210
F12_0102	1159.700	1162.700	6	33	1210
F12_0103	918.375	921.375	6	33	1210
			Total:		3630
CLNO0101	778.525	781.525	18	39	968
CLNO0102	1290.625	1293.625	15	39	1089
			Total:		2057
F11_0101	842.650	845.650	6	24	847
F11_0102	849.475	852.475	6	24	847
F11_0103	839.625	842.625	6	24	847
			Total:		2541
F22_0101	827.925	830.925	6	27	968
F22_0102	806.975	809.975	12	27	726
F22_0103	819.350	822.350	6	27	968
			Total:		2662
NH3_0101	964.650	967.650	6	21	726
NH3_0102	928.825	931.825	6	21	726
			Total:		1452
COF20101	772.000	775.000	15	36	968
COF20102	1225.750	1228.750	15	36	968
			Total:		1936
SF6_0101	946.625	949.625	6	21	726
SF6_0102	949.650	952.650	6	21	726
			Total:		1452
			Grand Total:		15730

4.4 Results by Species

In this section the results for each species are shown in more detail.

The microwindow plots show the wavenumber and altitude range (left scale) of the selected microwindows. Horizontal lines indicate the nominal MIPAS tangent altitudes. Superimposed (right scale) are the total radiance (grey) and absorber contribution (black) calculated for 12km tangent height in a mid-latitude day-time atmosphere, and the dashed line shows the NESR. No data are plotted for the MIPAS bandgaps (marked by vertical lines).

The retrieval accuracy plots show the profile used, with dashed and dotted lines indicating ±100% and ±30% error margins respectively. 100% is the *a priori* (random) error assumed for the microwindow selection, and 30% is considered the limit for 'useful' accuracy from a single profile retrieval. The horizontal lines show the predicted retrieval accuracy (i.e., total = random + systematic errors) using all selected microwindows. There are actually two pairs of vertical bars, the inner pair indicating precision (i.e. random error) but in most cases the two are indistinguishable since the random error is the dominant component.

Finally there is a tabulation of the microwindows in their selection sequence, giving both spectral and tangent altitude ranges, the total number of measurements (NPts) (= no. of spectral points × no. of tangent altitudes) and the number of 'unmasked' measurements which are actually used within the microwindow.

For HNO_4 and C_2H_2 no microwindows could be found but the spectral plots and assumed profiles are listed for information.

4.4.1 CFC-12

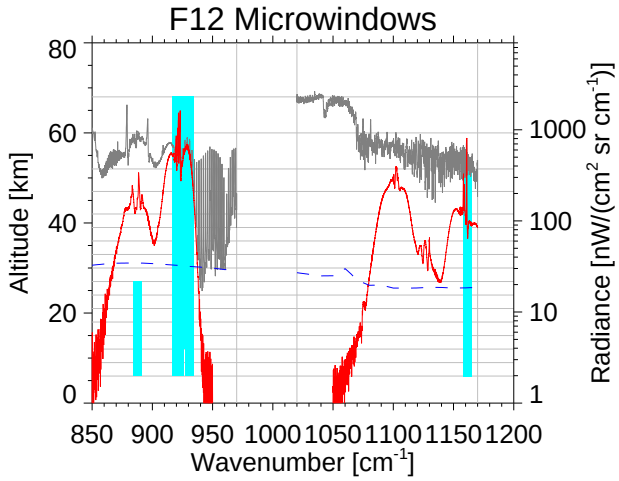

Figure 10: CFC-12 microwindows and spectrum.

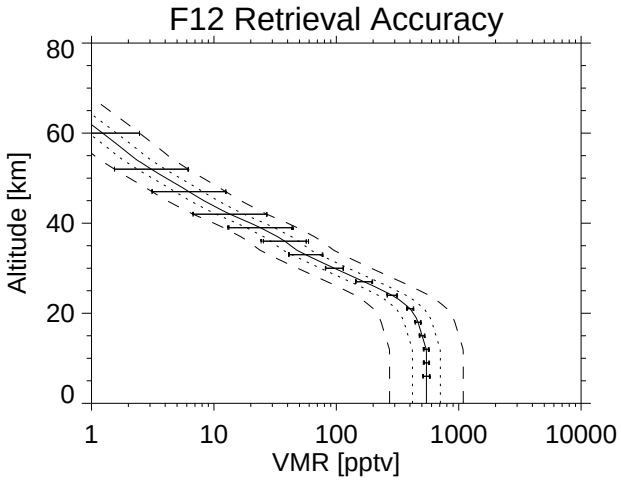

Figure 11: CFC-12 profile and retrieval errors

Table 11: CFC-12 Microwindows

MW	Waveno. Range		Alt.		NPts	NUse
1	921.400	924.400	6	68	2057	1158
2	1159.700	1162.700	6	52	1815	714
3	918.375	921.375	6	68	2057	1567
4	924.425	927.425	12	68	1815	1512
5	929.125	932.125	6	68	2057	1167
6	885.975	888.975	6	27	968	381
			Total:		10769	6499

4.4.2 CFC-14

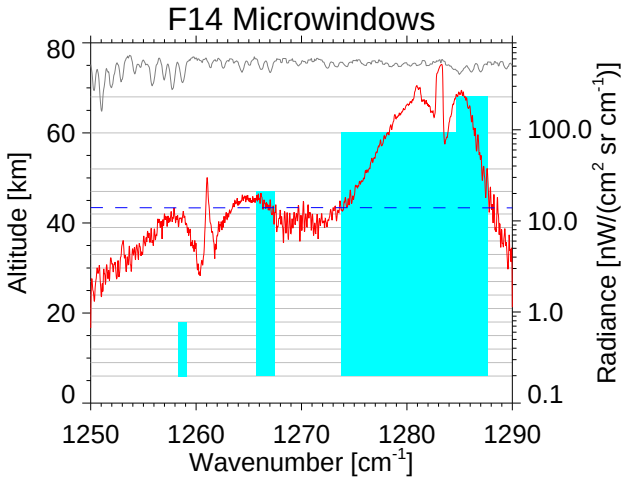

Figure 12: CFC-14 microwindows and spectrum.

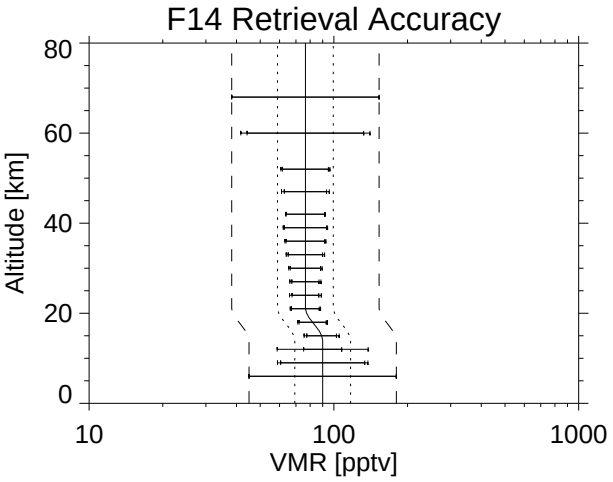

Figure 13: CFC-14 profile and retrieval errors

Table 12: CFC-14 Microwindows

MW	Waveno. Range		Alt.		NPts	NUse
1	1281.625	1284.625	6	60	1936	1256
2	1284.650	1287.650	6	68	2057	1479
3	1278.600	1281.600	6	60	1936	899
4	1273.800	1276.800	6	60	1936	1098
5	1276.825	1278.575	6	60	1136	555
6	1265.750	1267.475	6	47	980	678
7	1258.300	1259.025	6	18	150	89
			Total:		10131	6054

4.4.3 $ClONO_2$

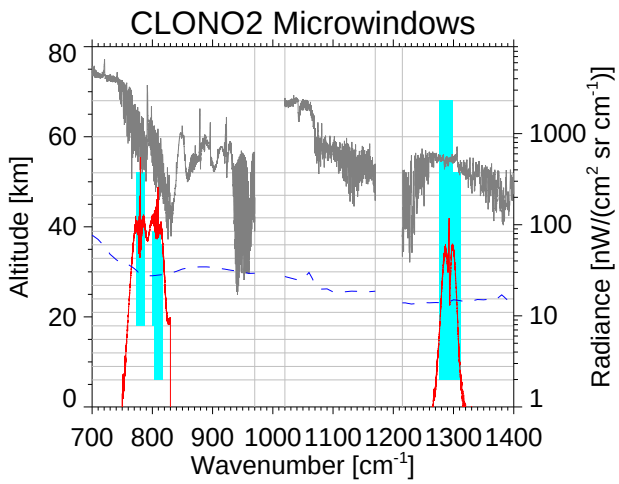

Figure 14: $ClONO_2$ microwindows and spectrum.

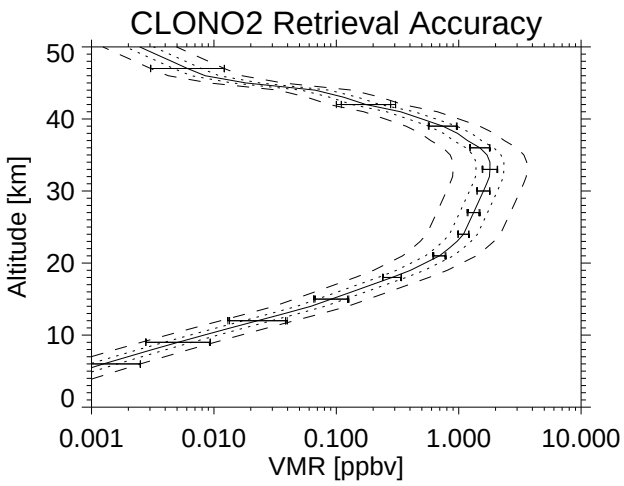

Figure 15: $ClONO_2$ profile and retrieval errors

Table 13: $ClONO_2$ Microwindows

MW	Waveno. Range		Alt.		NPts	NUse
1	778.525	781.525	18	52	1331	836
2	1290.625	1293.625	6	68	2057	1046
3	808.425	811.425	6	36	1331	436
4	1303.350	1306.350	6	52	1815	1124
5	805.400	808.400	18	39	968	565
6	1285.025	1286.550	6	42	806	415
7	1282.125	1285.000	6	68	1972	1085
				Total:	10280	5507

4.4.4 CFC-11

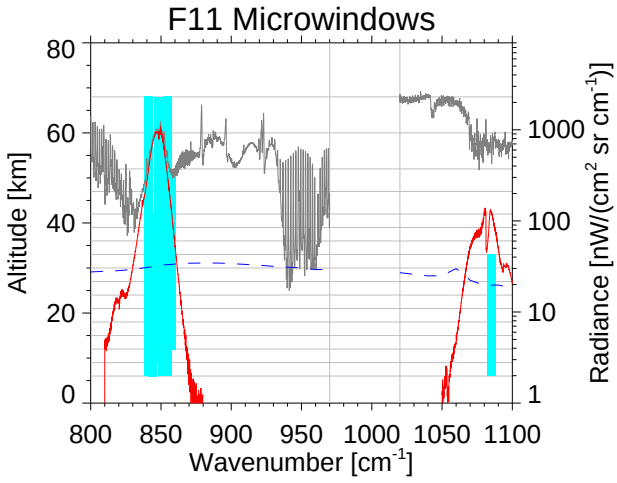

Figure 16: CFC-11 microwindows and spectrum.

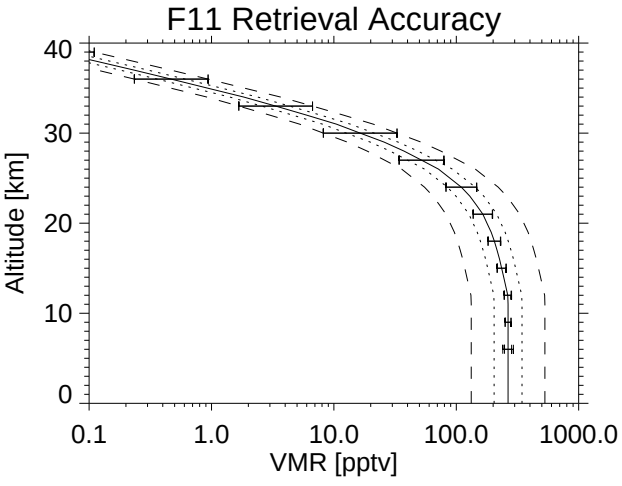

Figure 17: CFC-11 profile and retrieval errors

Table 14: CFC-11 Microwindows

MW	Waveno. Range		Alt.		NPts	NUse
1	842.650	845.650	6	42	1573	1402
2	849.475	852.475	6	39	1452	909
3	839.625	842.625	6	68	2057	1384
4	853.075	856.075	6	68	2057	796
5	846.450	849.450	9	68	1936	1308
6	1084.575	1085.875	6	33	530	260
7	856.250	859.250	12	52	1573	927
				Total:	11178	6986

4.4.5 HCFC-22

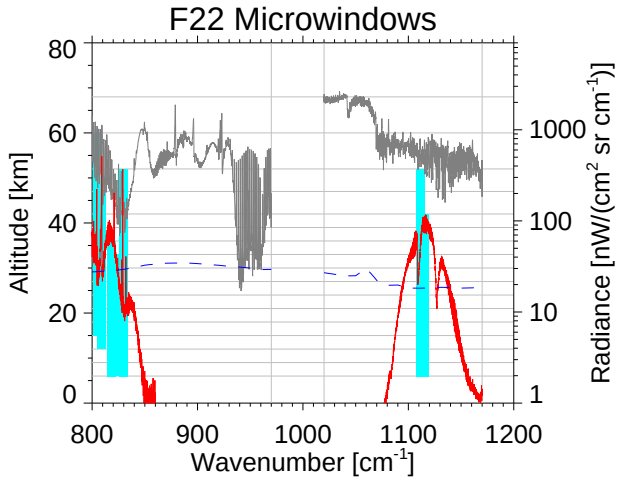

Figure 18: HCFC-22 microwindows and spectrum.

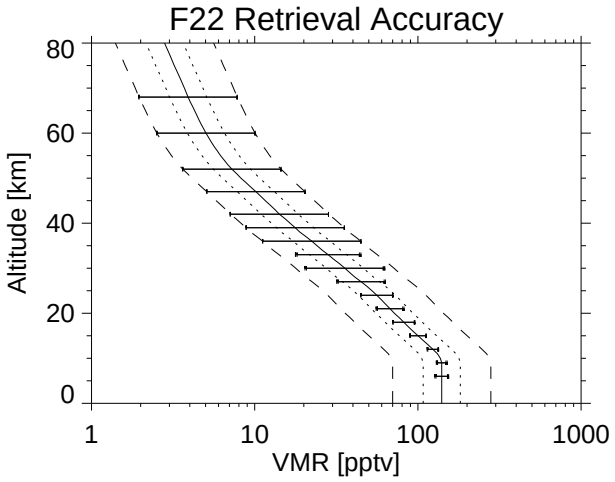

Figure 19: HCFC-22 profile and retrieval errors

Table 15: HCFC-22 Microwindows

MW	Waveno. Range		Alt.		NPts	NUse
1	827.925	830.925	6	52	1815	1171
2	806.975	809.975	12	47	1452	686
3	819.350	822.350	6	33	1210	923
4	1113.525	1116.500	6	42	1560	485
5	803.575	806.575	15	60	1573	881
6	1110.250	1113.250	6	52	1815	870
7	817.150	819.325	6	36	968	542
				Total:	10393	5558

4.4.6 NH_3

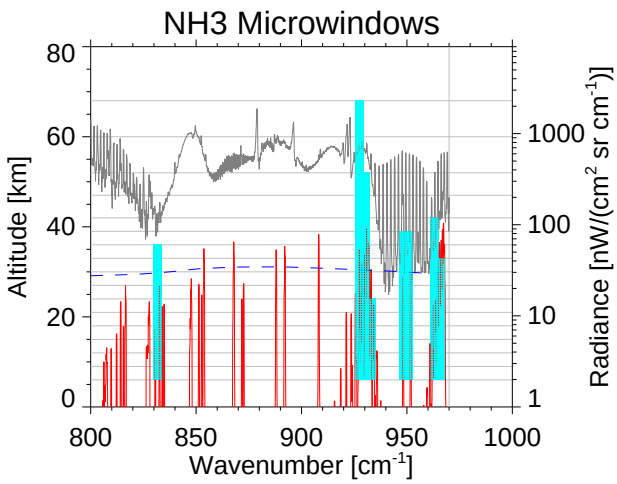

Figure 20: NH_3 microwindows and spectrum.

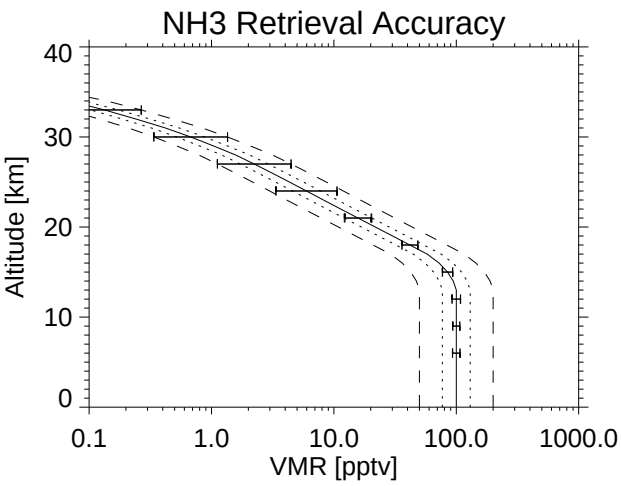

Figure 21: NH_3 profile and retrieval errors

Table 16: NH_3 Microwindows

MW	Waveno. Range		Alt.		NPts	NUse
1	964.650	967.650	6	33	1210	806
2	928.825	931.825	6	52	1815	1570
3	949.350	952.175	6	39	1368	652
4	961.625	964.625	6	42	1573	823
5	947.600	949.150	6	39	756	274
6	926.075	928.800	6	68	1870	1205
7	830.425	833.425	6	36	1331	508
8	931.850	934.850	6	24	847	441
				Total:	10770	6279

4.4.7 HCN

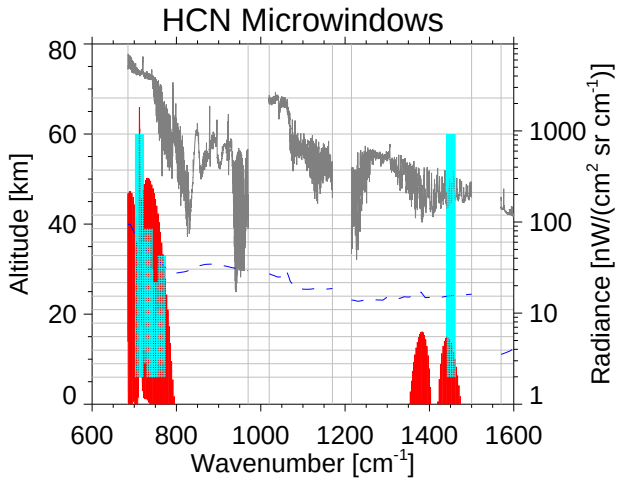

Figure 22: HCN microwindows and spectrum.

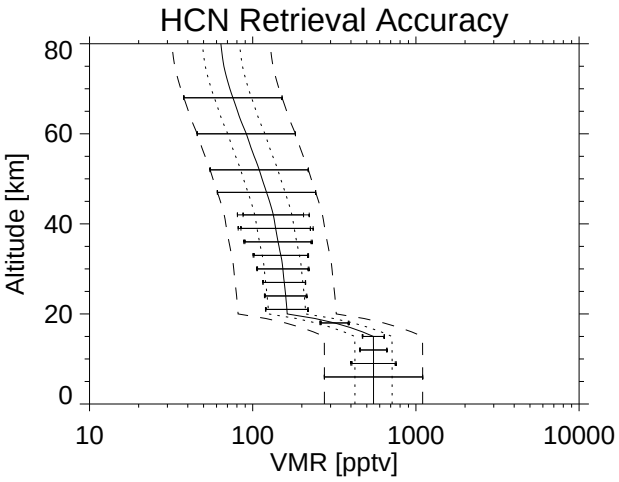

Figure 23: HCN profile and retrieval errors

Table 17: HCN Microwindows

MW	Waveno. Range		Alt.		NPts	NUse
1	711.125	714.125	6	60	1936	995
2	744.300	744.525	6	18	50	43
3	761.950	762.225	9	21	60	33
4	735.450	735.775	18	30	70	36
5	746.775	747.825	6	27	344	117
6	732.375	732.975	9	39	275	115
7	764.950	765.325	6	33	160	61
8	1450.325	1451.900	6	60	1024	503
9	726.450	726.825	12	36	144	60
10	738.450	738.800	6	21	90	53
				Total:	4153	2016

4.4.8 COF_2

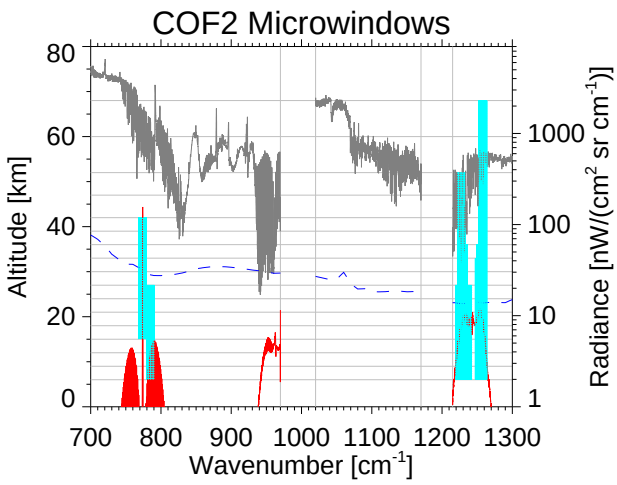

Figure 24: COF_2 microwindows and spectrum.

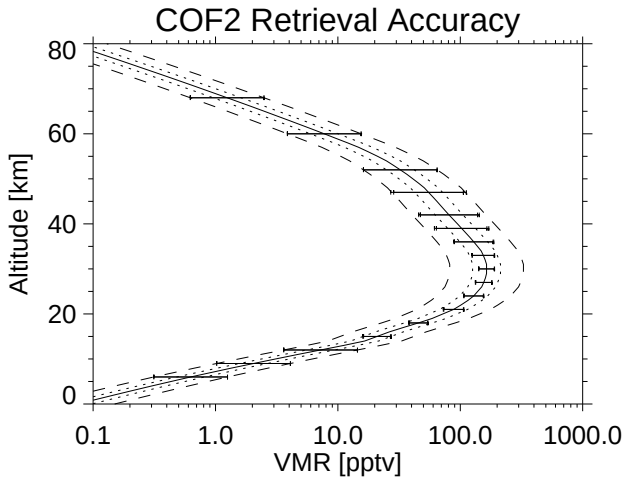

Figure 25: COF_2 profile and retrieval errors

Table 18: COF_2 Microwindows

MW	Waveno. Range		Alt.		NPts	NUse
1	772.000	775.000	15	42	1210	728
2	1225.750	1228.750	15	52	1452	1172
3	1223.925	1225.100	6	27	384	278
4	1230.325	1231.325	9	36	410	327
5	1253.350	1255.575	6	36	990	341
6	1228.900	1230.275	6	30	504	298
7	1256.625	1259.625	6	68	2057	1130
8	784.425	785.275	6	27	280	111
9	1236.450	1237.250	6	27	264	130
10	1252.600	1253.250	6	33	270	160
				Total:	7821	4675

4.4.9 OCS

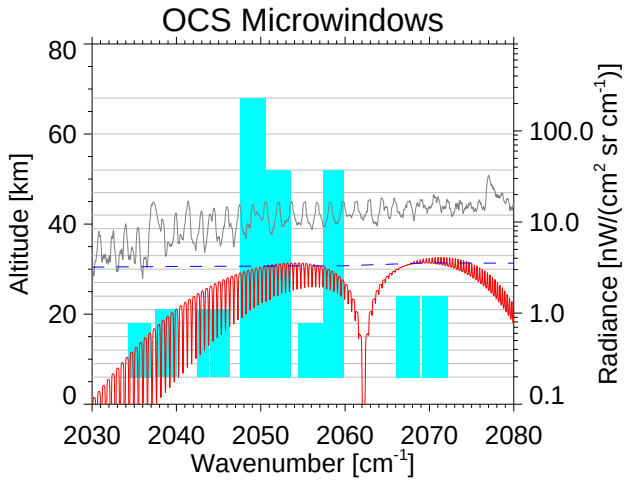

Figure 26: OCS microwindows and spectrum.

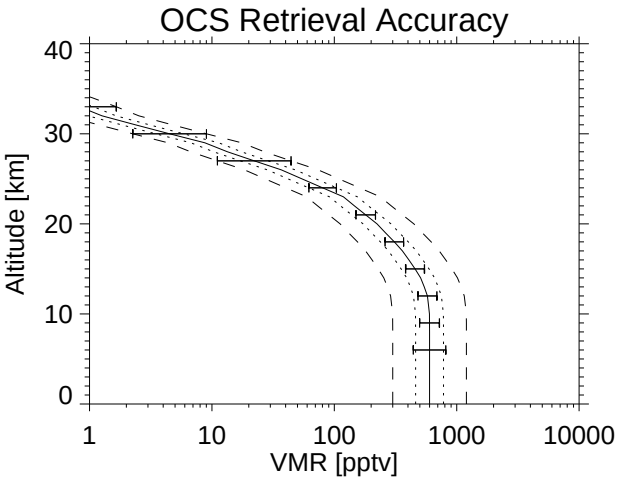

Figure 27: OCS profile and retrieval errors

Table 19: OCS Microwindows

MW	Waveno. Range		Alt.		NPts	NUse
1	2050.650	2053.575	6	52	1770	1315
2	2034.275	2036.925	6	18	535	380
3	2054.425	2057.425	6	18	605	480
4	2043.975	2046.325	6	21	570	420
5	2047.625	2050.625	6	68	2057	1210
6	2057.450	2059.875	6	52	1470	929
7	2037.475	2040.025	6	21	618	405
8	2066.025	2068.800	6	24	784	512
9	2042.475	2043.900	6	21	348	160
10	2069.150	2072.150	6	24	847	418
				Total:	9604	6229

4.4.10 SF_6

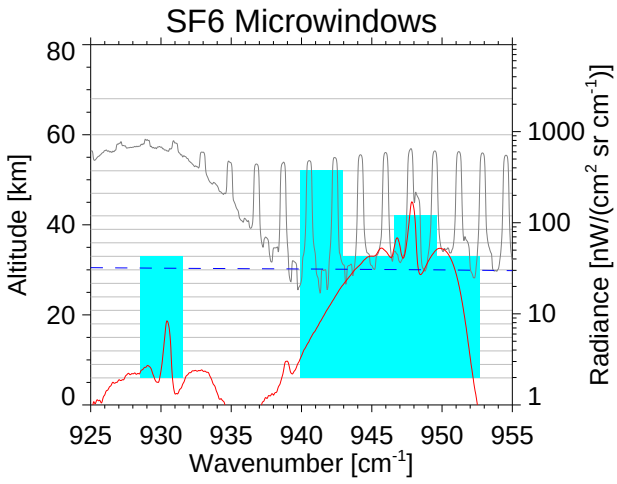

Figure 28: SF_6 microwindows and spectrum.

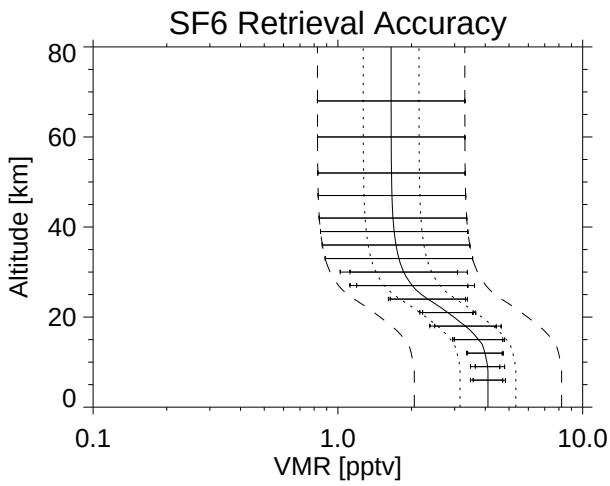

Figure 29: SF_6 profile and retrieval errors

Table 20: SF_6 Microwindows

MW	Waveno. Range		Alt.		NPts	NUse
1	946.625	949.625	6	42	1573	1359
2	949.650	952.650	6	33	1210	1043
3	942.975	945.975	6	33	1210	967
4	939.950	942.950	6	52	1815	602
5	946.000	946.600	6	33	250	203
6	928.525	931.525	6	33	1210	563
				Total:	7268	4737

4.4.11 N_2O_5

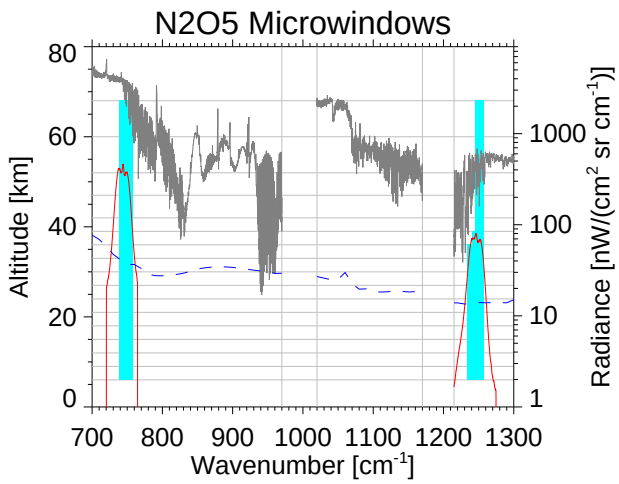

Figure 30: N_2O_5 microwindows and spectrum.

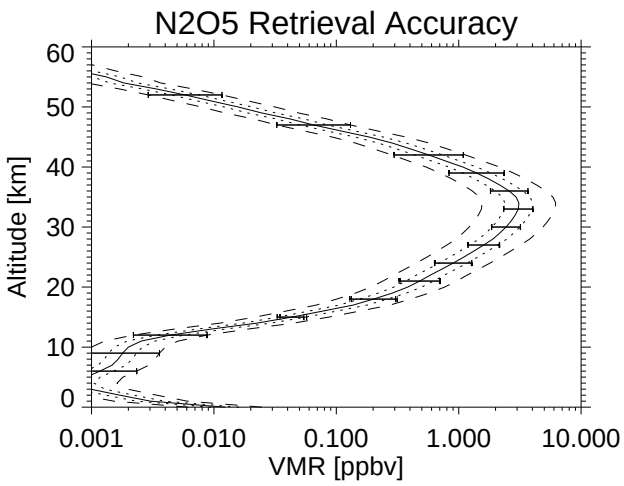

Figure 31: N_2O_5 profile and retrieval errors

Table 21: N_2O_5 Microwindows

MW	Waveno. Range		Alt.		NPts	NUse
1	750.650	753.350	6	68	1853	1033
2	742.900	745.900	6	68	2057	889
3	1238.825	1241.775	6	36	1309	633
4	1245.675	1248.675	6	39	1452	923
5	746.100	749.100	6	52	1815	938
6	1249.675	1252.675	6	68	2057	1164
			Total:		10543	5580

4.4.12 C_2H_6

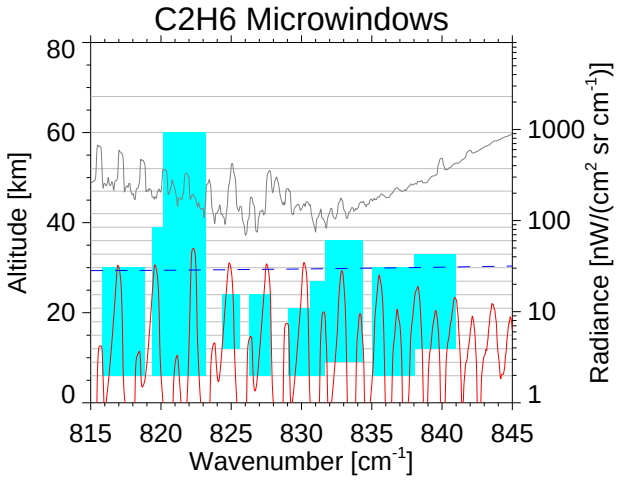

Figure 32: C_2H_6 microwindows and spectrum.

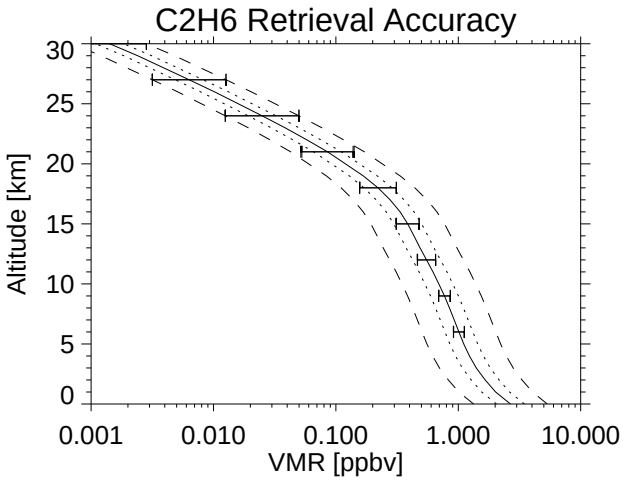

Figure 33: C_2H_6 profile and retrieval errors

Table 22: C_2H_6 Microwindows

MW	Waveno. Range		Alt.		NPts	NUse
1	820.200	823.200	6	60	1936	677
2	815.825	818.825	6	30	1089	486
3	831.650	834.350	9	36	1090	655
4	819.350	820.175	6	39	408	200
5	829.025	830.575	6	21	378	195
6	838.050	840.975	12	33	944	351
7	835.025	838.025	6	30	1089	576
8	826.325	827.825	6	24	427	189
9	824.375	825.600	12	24	250	128
10	830.600	831.625	6	27	336	195
			Total:		7947	3652

4.4.13 HOCl

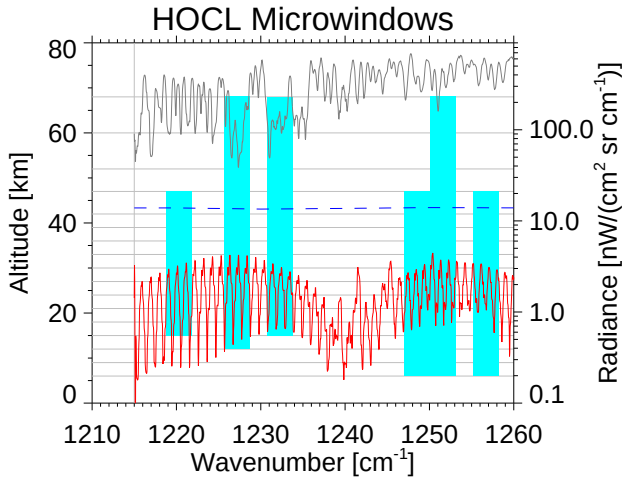

Figure 34: HOCl microwindows and spectrum.

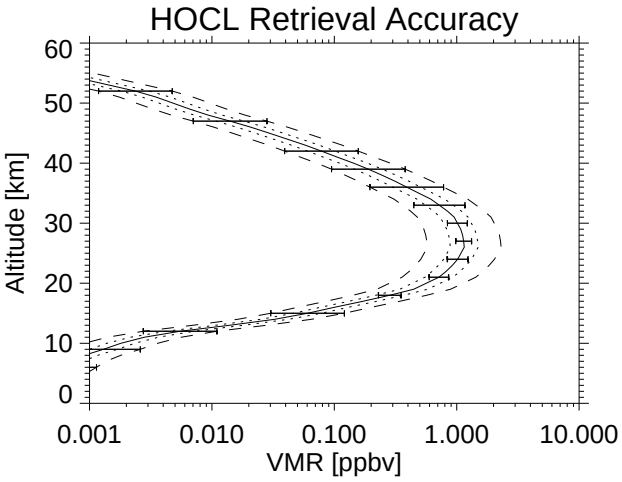

Figure 35: HOCl profile and retrieval errors

Table 23: HOCl Microwindows

MW	Waveno. Range		Alt.		NPts	NUse
1	1225.725	1228.725	12	68	1815	1342
2	1230.775	1233.775	15	68	1694	1319
3	1250.150	1253.150	6	68	2057	1143
4	1255.250	1258.250	6	47	1694	963
5	1218.775	1221.775	15	47	1331	555
6	1247.050	1250.050	6	47	1694	891
				Total:	10285	6213

4.4.14 SO_2

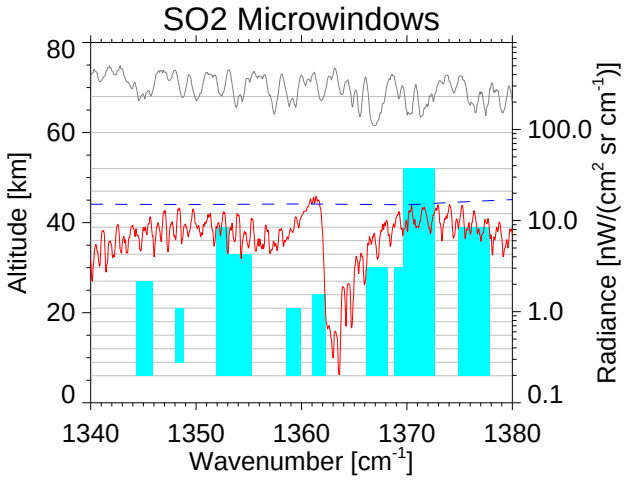

Figure 36: SO_2 microwindows and spectrum.

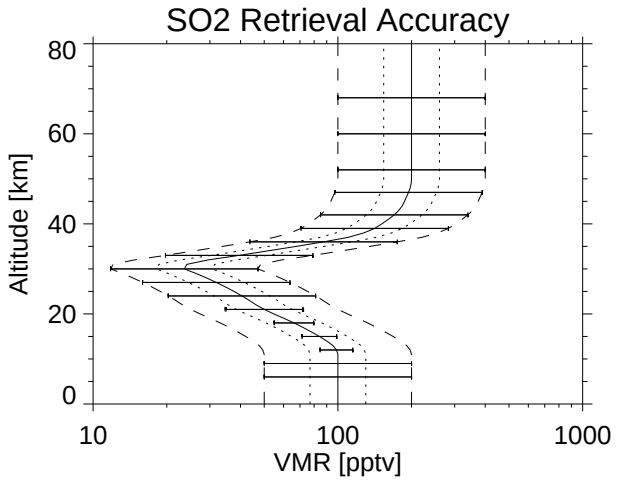

Figure 37: SO_2 profile and retrieval errors

Table 24: SO_2 Microwindows

MW	Waveno. Range		Alt.		NPts	NUse
1	1369.675	1372.675	6	52	1815	1087
2	1361.025	1362.350	6	24	378	243
3	1366.100	1368.150	6	30	747	581
4	1353.150	1355.325	6	33	880	435
5	1374.850	1377.850	6	39	1452	863
6	1348.150	1348.700	9	21	115	110
7	1358.575	1359.950	6	21	336	147
8	1351.875	1353.050	6	39	576	308
9	1368.875	1369.500	6	30	234	168
10	1344.350	1345.925	6	27	512	293
				Total:	7045	4235

4.4.15 H_2O_2

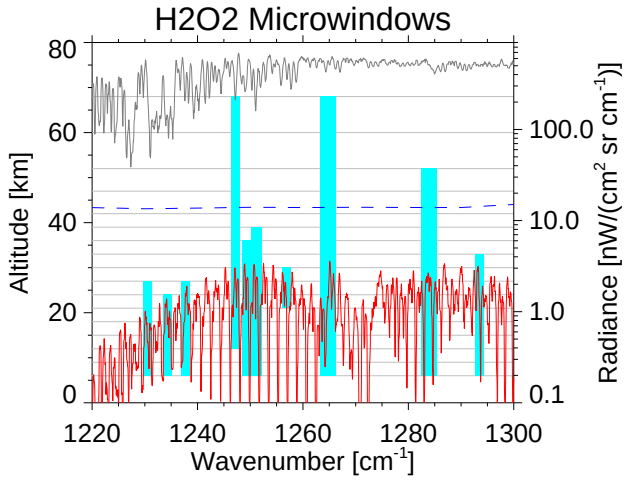

Figure 38: H_2O_2 microwindows and spectrum.

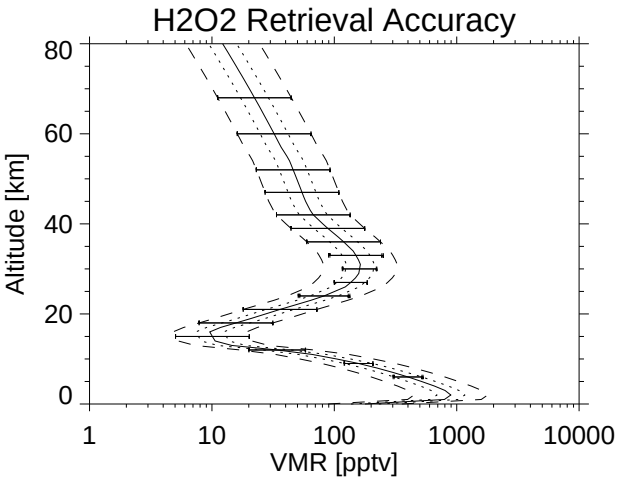

Figure 39: H_2O_2 profile and retrieval errors

Table 25: H_2O_2 Microwindows

MW	Waveno. Range		Alt.		NPts	NUse
1	1233.425	1235.075	6	24	469	283
2	1246.900	1247.475	12	68	360	324
3	1250.125	1252.125	6	39	972	402
4	1248.750	1249.650	6	36	407	233
5	1256.625	1257.125	21	30	84	64
6	1229.625	1231.275	6	27	536	348
7	1263.325	1266.325	6	68	2057	1033
8	1292.750	1294.250	6	33	610	285
9	1282.450	1285.450	6	52	1815	785
10	1237.400	1237.975	6	27	192	114
			Total:		7502	3871

4.4.16 ClO

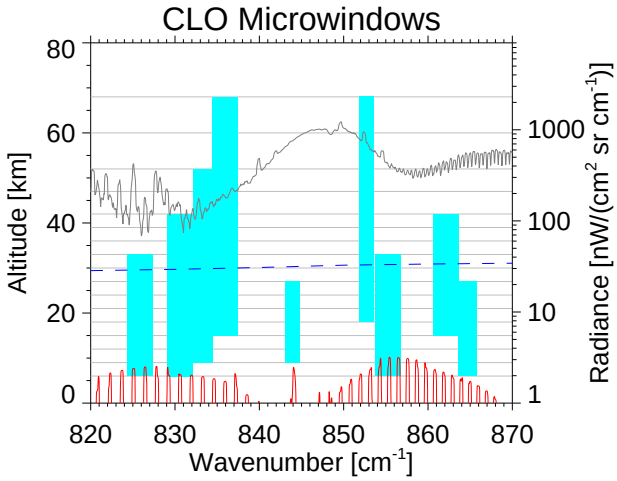

Figure 40: ClO microwindows and spectrum.

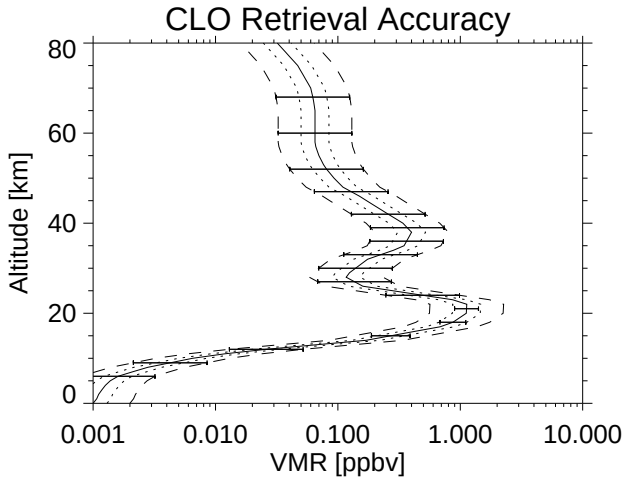

Figure 41: ClO profile and retrieval errors

Table 26: ClO Microwindows

MW	Waveno. Range		Alt.		NPts	NUse
1	829.100	832.100	6	42	1573	865
2	834.425	837.425	15	68	1694	1400
3	853.750	856.750	6	33	1210	686
4	851.875	853.575	18	68	897	755
5	832.125	834.400	9	52	1288	709
6	860.625	863.625	15	42	1210	671
7	824.375	827.350	6	33	1200	606
8	863.650	865.800	6	27	696	294
9	843.025	844.750	9	27	490	236
			Total:		10258	6222

4.4.17 CCl_4

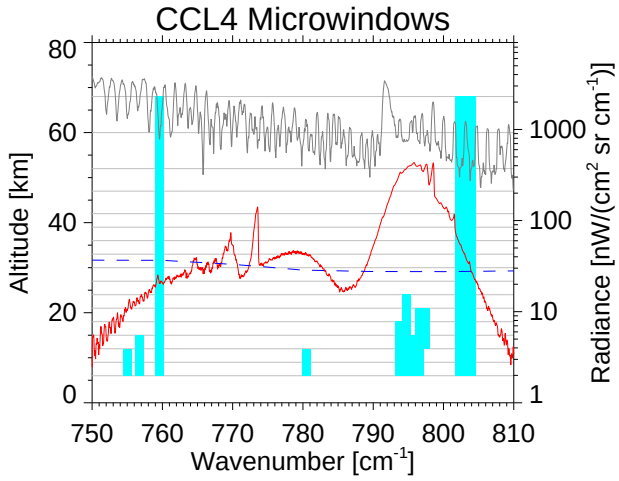

Figure 42: CCl_4 microwindows and spectrum.

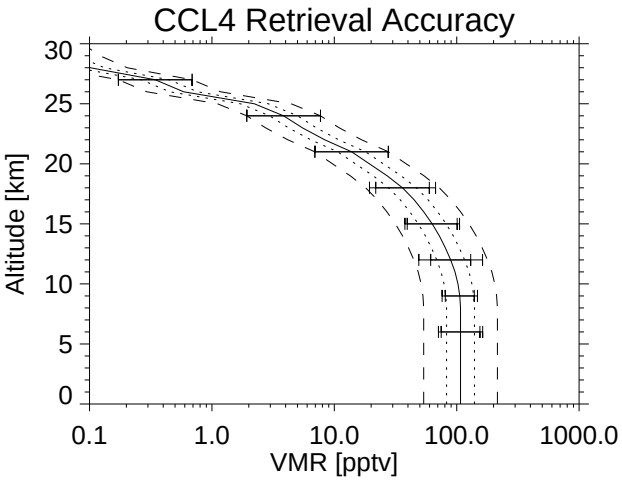

Figure 43: CCl_4 profile and retrieval errors

Table 27: CCl_4 Microwindows

MW	Waveno.	Range	Alt.		NPts	NUse
1	794.225	795.275	6	24	301	142
2	796.425	796.825	6	21	102	51
3	797.150	797.600	12	21	76	52
4	780.400	780.625	6	12	30	16
5	754.775	755.175	6	12	51	30
6	795.700	796.125	6	15	72	46
7	793.525	793.825	6	18	65	35
8	756.625	757.000	6	15	64	44
9	801.600	804.575	6	68	2040	777
10	759.225	760.025	6	68	561	319
			Total:		3362	1512

4.4.18 HNO_4

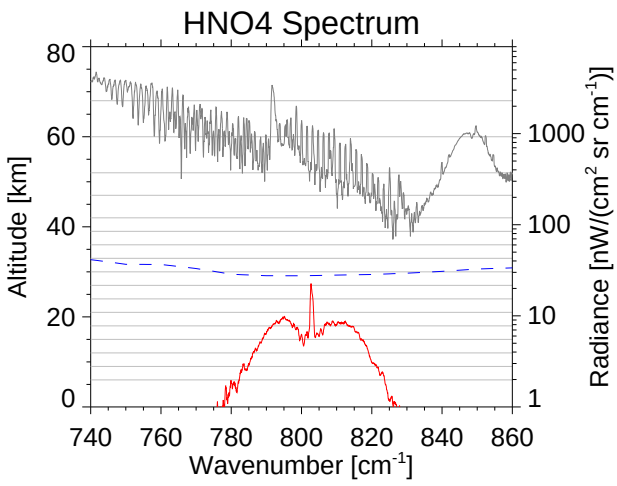

Figure 44: HNO_4 spectrum.

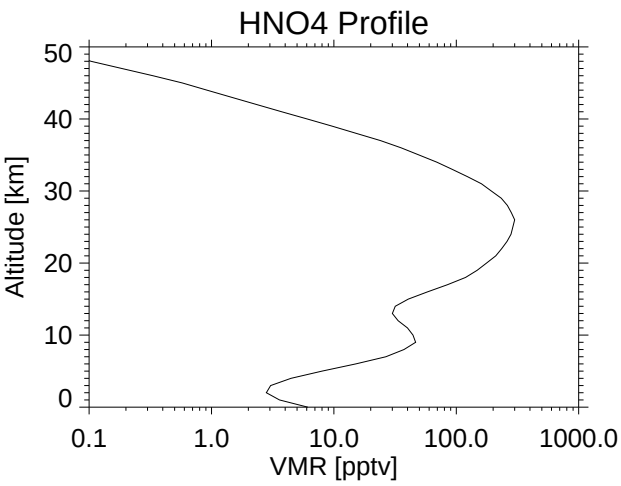

Figure 45: HNO_4 profile

No microwindows were found for HNO_4.

4.4.19 C_2H_2

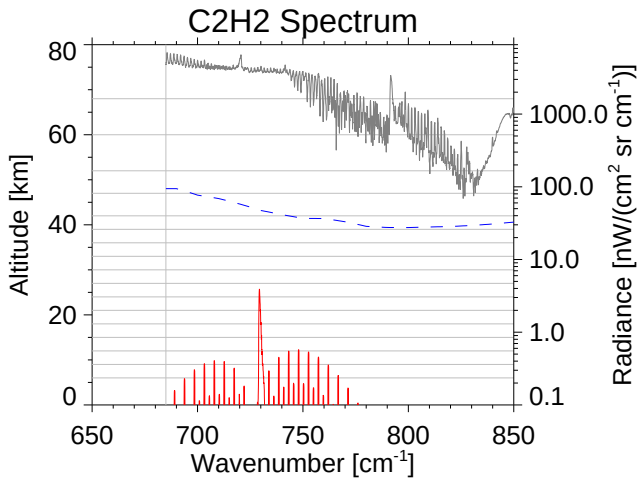

Figure 46: C_2H_2 spectrum.

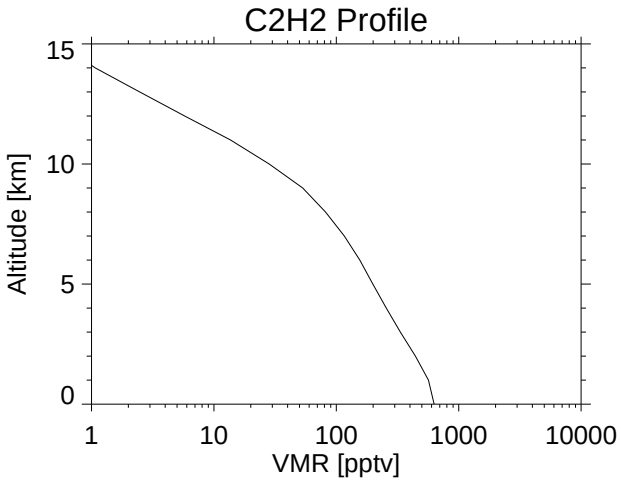

Figure 47: C_2H_2 profile

No microwindows were found for C_2H_2.

4.5 Spectroscopic Errors

Spectroscopic database errors for the additional species have not been considered as part of the microwindow selection. However, results from a parallel study[29], summarised in Table 28, have been incorporated retrospectively to predict the information loss represented by this additional error.

There are arguments for regarding spectroscopic errors as either correlated or uncorrelated between microwindows, but here it is assumed that they are *uncorrelated*. For example, it is assumed that the error in NH_3 line strengths is randomly distributed between microwindows with a standard deviation of 15%, rather than all NH_3 lines having the same, but unknown, error with 1-σ uncertainty $\pm 15\%$. (For the particular case of line strength uncertainties, a *fully correlated* error would translate directly into the error in retrieved concentration).

Table 28: Estimate of the information loss (in 'bits') for retrievals of minor species as a result of current uncertainties in spectroscopic parameters: line position ν, strength I and halfwidth γ.

Molecule	$\delta\nu$ $[10^{-3}\text{cm}^{-1}]$	$\delta I/I$ [%]	$\delta\gamma/\gamma$ [%]	Δ Info [bits]
C_2H_6	-	50	-	−6.6
NH_3	1	15	20	−0.3
HCN	3	10	15	−0.3
COF_2	1	5	10	−0.2
HOCl	1	4	10	−0.07
ClO	0.5	10	15	−0.04
OCS	0.5	6	15	−0.04
SO_2	10	20	30	−0.07
H_2O_2	2	8	25	−0.02

In most cases it can be seen that the contribution of spectroscopic errors to the total error is small. However this is generally because the total error is dominated by the random (S/N) rather than the systematic component. Nevertheless, spectroscopic uncertainties can contribute a significant fraction of the systematic error, as shown in the following plots.

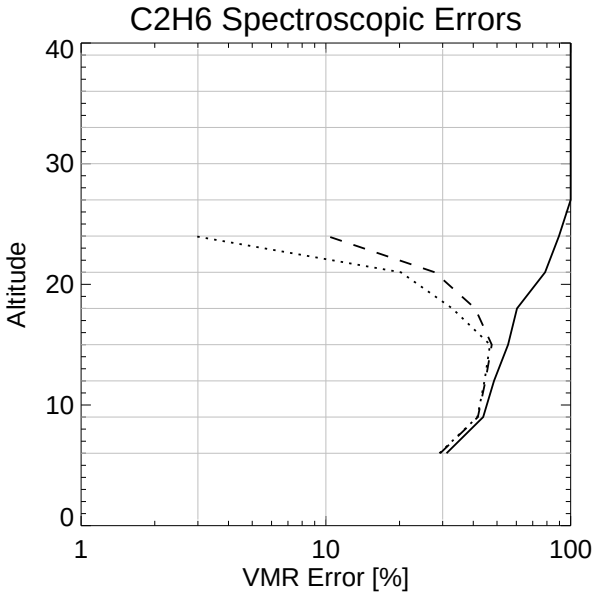

Figure 48: Contribution of spectroscopic database uncertainties (dotted line) to overall systematic error (dashed line) and total error (solid line) for a C_2H_6 retrieval.

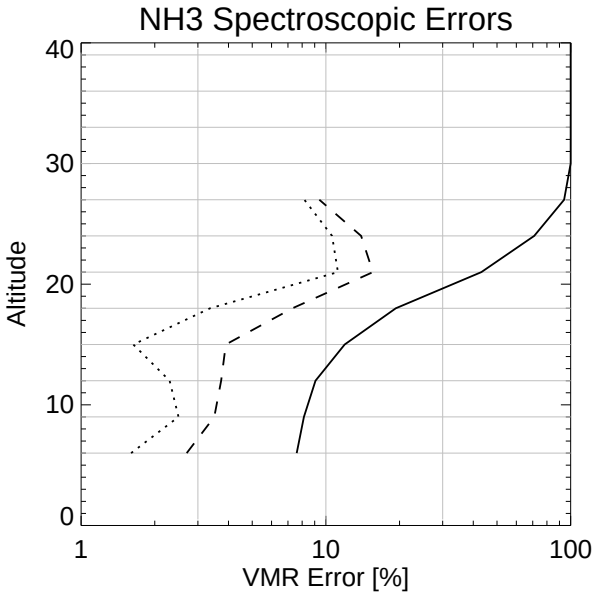

Figure 49: Contribution of spectroscopic database uncertainties (dotted line) to overall systematic error (dashed line) and total error (solid line) for a NH_3 retrieval.

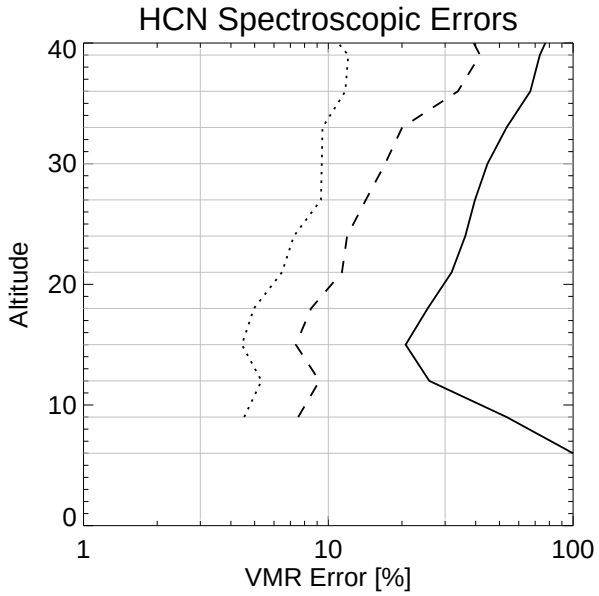

Figure 50: Contribution of spectroscopic database uncertainties (dotted line) to overall systematic error (dashed line) and total error (solid line) for a HCN retrieval.

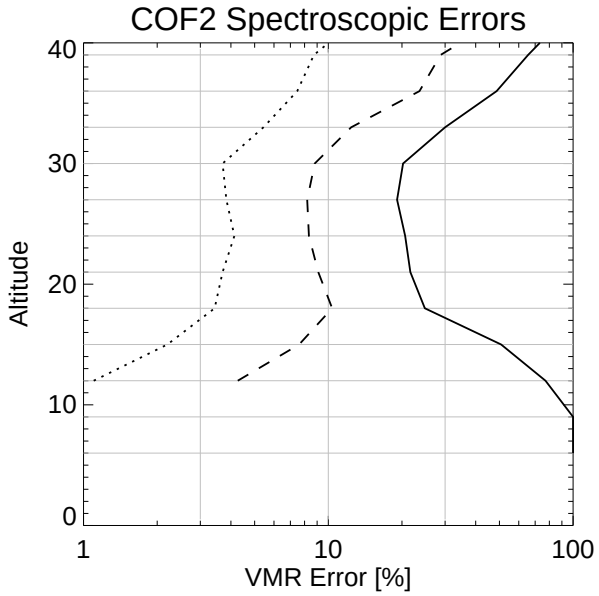

Figure 51: Contribution of spectroscopic database uncertainties (dotted line) to overall systematic error (dashed line) and total error (solid line) for a COF_2 retrieval.

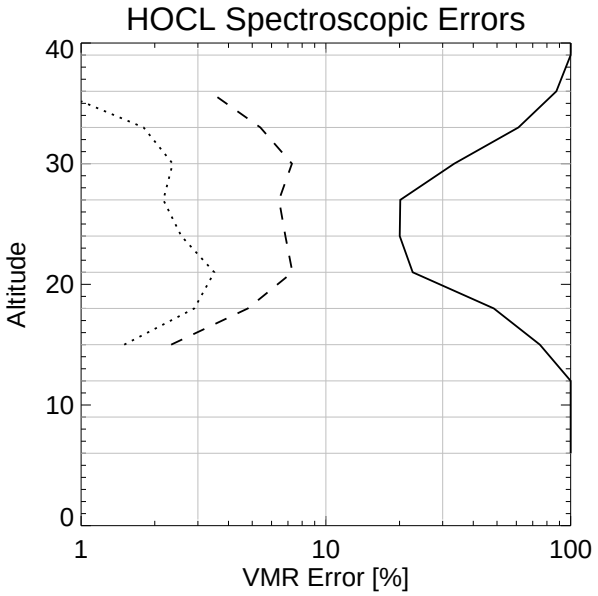

Figure 52: Contribution of spectroscopic database uncertainties (dotted line) to overall systematic error (dashed line) and total error (solid line) for a HOCl retrieval.

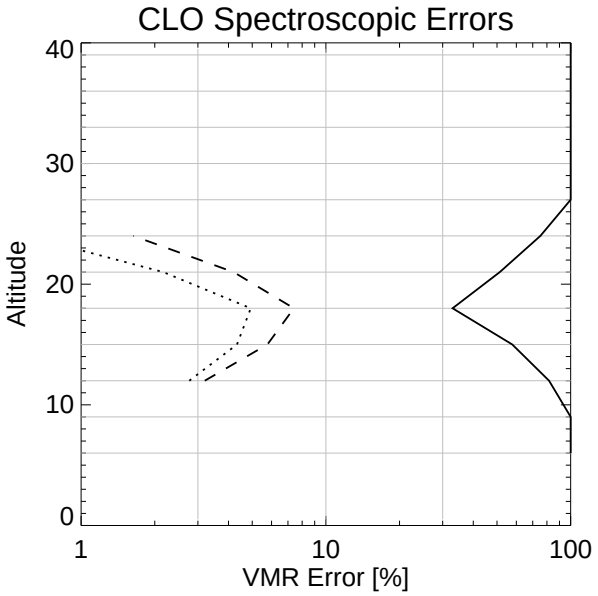

Figure 53: Contribution of spectroscopic database uncertainties (dotted line) to overall systematic error (dashed line) and total error (solid line) for a ClO retrieval.

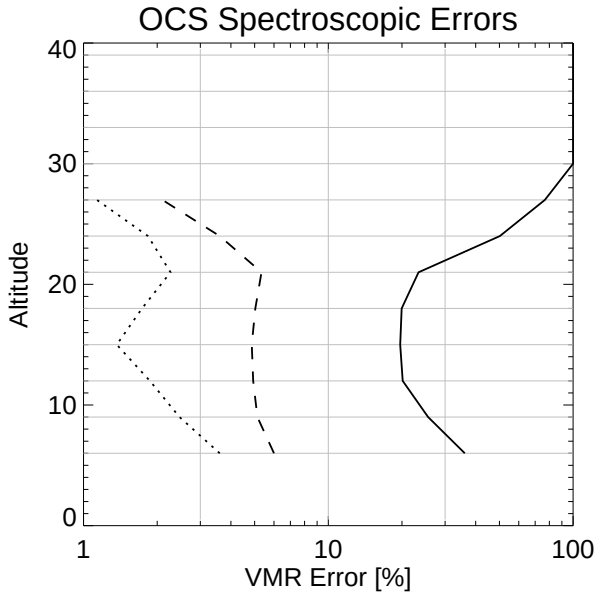

Figure 54: Contribution of spectroscopic database uncertainties (dotted line) to overall systematic error (dashed line) and total error (solid line) for a OCS retrieval.

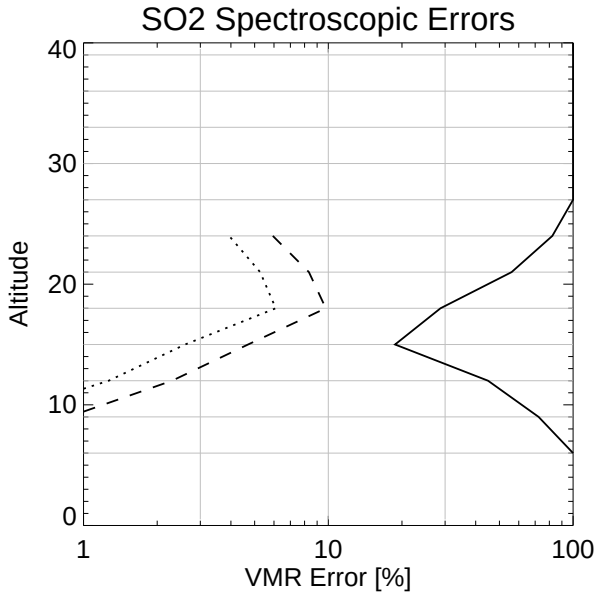

Figure 55: Contribution of spectroscopic database uncertainties (dotted line) to overall systematic error (dashed line) and total error (solid line) for a SO_2 retrieval.

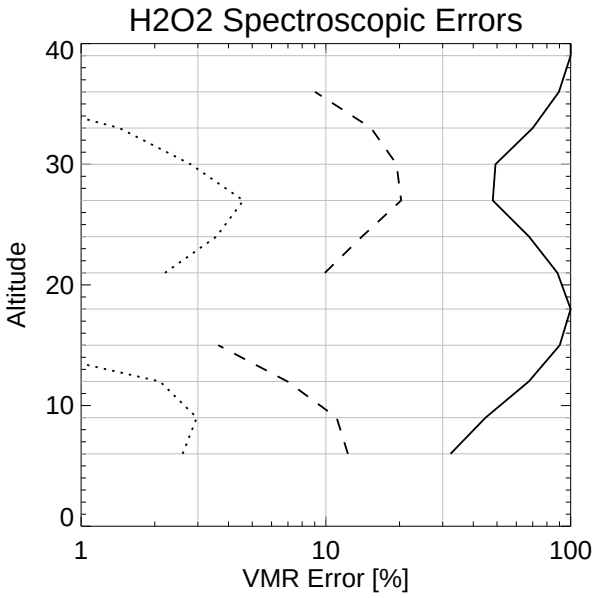

Figure 56: Contribution of spectroscopic database uncertainties (dotted line) to overall systematic error (dashed line) and total error (solid line) for a H_2O_2 retrieval.

4.6 Special Cases

In this section three additional molecules are considered which require some modification to the current operational retrieval algorithm: CO, NO and CO_2.

4.6.1 CO

CO emissions in the infrared are strongly influenced by non-LTE processes, particularly at high altitude and in the day-time, although CO itself does not have any significant diurnal variation in concentration. This suggests that a nighttime LTE retrieval might be feasible when the non-LTE effects are small enough to be ignored (corresponding to option 1 in section 1.7). Alternatively, since CO is a relatively simple molecule, the non-LTE emission may be closely approximated by a single 'vibrational temperature' profile. In principle, therefore, a joint-microwindow selection could be performed to retrieve both CO and its vibrational temperature (option 4 in section 1.7). The question is whether it is possible to discriminate between in the two spectral signatures, i.e., whether the respective Jacobians are distinct.

Microwindows selected for the two cases are listed in Tables 29 and 30 and plotted in Figs. 57 and 58. In both cases the limit of 10000 measurements restricts the number of microwindows selected.

Table 29: CO nighttime (LTE) Microwindows

MW	Waveno. Range		Alt.		NPts	NUse
1	2138.575	2141.525	6	68	2023	1671
2	2156.025	2159.025	6	68	2057	1772
3	2150.200	2153.200	6	52	1815	1333
4	2054.925	2057.925	6	68	2057	968
5	2133.900	2136.900	6	42	1573	1340
6	2110.175	2113.125	6	27	952	632
				Total:	10477	7716

Table 30: Joint CO, T_{vib} day-time (non-LTE) Microwindows

MW	Waveno. Range		Alt.		NPts	NUse
1	2157.675	2160.650	6	68	2040	2040
2	2133.875	2135.725	6	68	1275	1274
3	2111.200	2111.975	6	68	544	544
4	2055.250	2058.250	6	68	2057	1392
5	2138.825	2141.825	6	68	2057	1893
6	2145.725	2148.725	6	68	2057	1732
				Total:	10030	8875

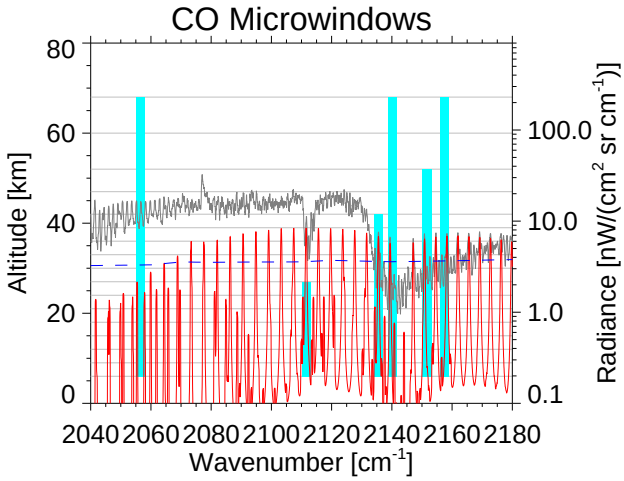

Figure 57: CO nighttime (LTE) microwindows and the CO spectrum.

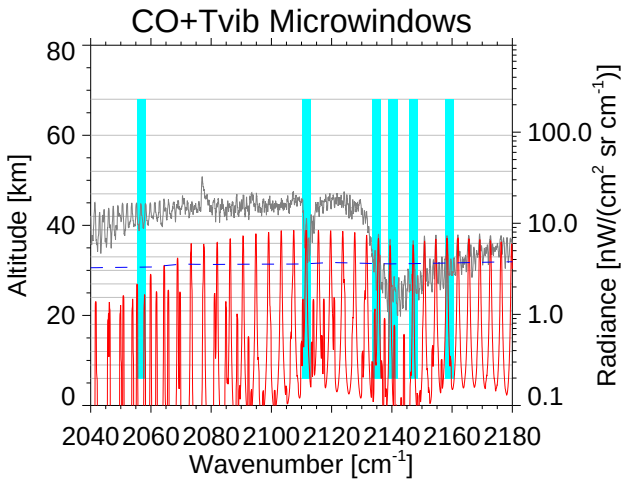

Figure 58: Joint CO, T_{vib} day-time (non-LTE) microwindows and the CO spectrum.

Fig. 59 shows the CO profile and expected accuracy for the LTE case, and Fig. 60 the (kinetic−vibrational) temperature profile and expected accuracy for the non-LTE case. Results are summarised in Fig. 61.

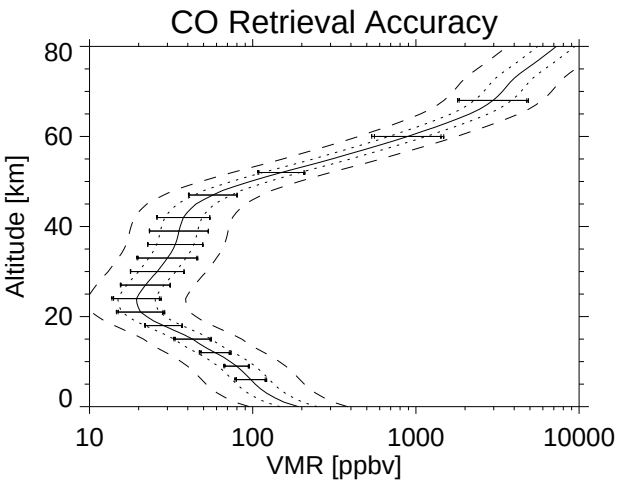

Figure 59: CO profile and retrieval errors for a mid-latitude night-time scenario assuming LTE. The dashed lines represent the ±100% *a priori* uncertainty and the dotted lines the ±30% limit of 'useful' accuracy. Inner ticks on error bars are precision, outer ticks are accuracy.

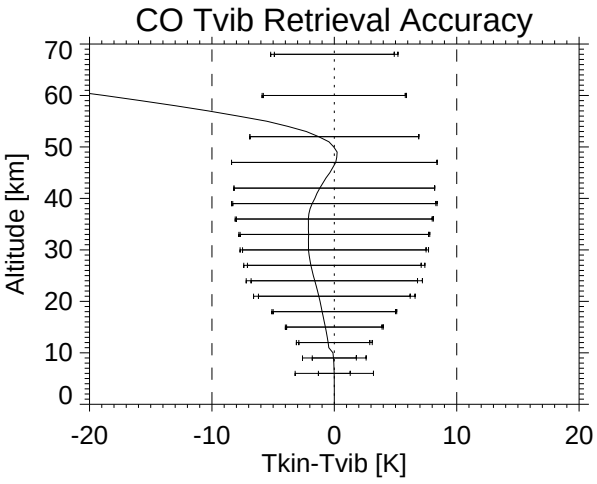

Figure 60: Difference between the kinetic and vibrational temperatures, and retrieval errors for mid-latitude day-time scenario assuming a joint CO,T_{vib} retrieval. The dashed lines represent the ±10 K *a priori* retrieval uncertainty.

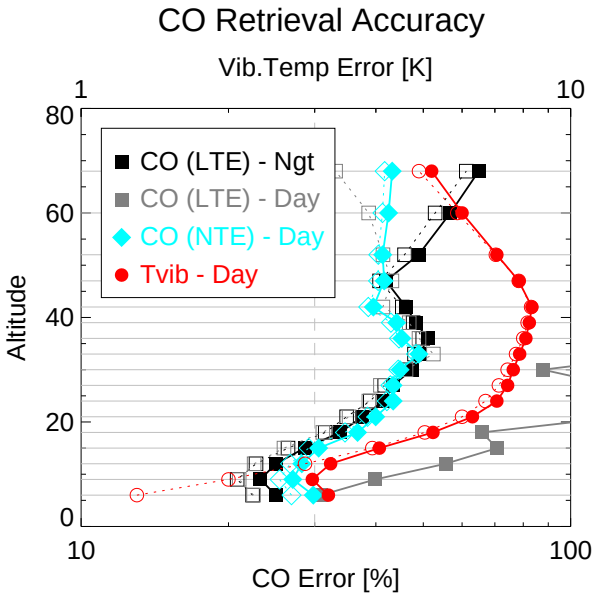

Figure 61: Retrieval accuracy profiles for CO assuming LTE in nighttime and daytime scenarios, and for CO (NTE) jointly with T_{vib} (top axis) in the daytime. Solid symbols/lines are accuracy, open symbols/dashed lines are precision.

From Fig. 61 it can be seen that the day-time non-LTE retrieval is slightly worse than the night-time LTE retrieval from 6–24 km, altitude, but both are capable of giving accuracy better than 30%. From 27–47 km results are comparable and, while the NTE retrieval is better above 47 km, the accuracy (40%) is probably not useful. However, for both cases the accuracy is limited by precision (i.e., S/N) and, given the regularity of the CO spectrum, it should be possible to improve on this by adding further (possibly narrower) microwindows.

Fig. 61 also shows the accuracy that would result if the LTE microwindows were used during the day-time, clearly illustrating that non-LTE effects cannot be ignored during the day-time.

The conclusion is that CO can be retrieved to useful accuracy in below 25 km either at nighttime (ignoring non-LTE effects) or in the day-time including a vibrational temperature retrieval. However, because of the wide spacing of CO lines and low MIPAS S/N in the the D-band, a relatively large number of microwindows/measurements (therefore high CPU cost) would be required.

4.6.2 NO

NO emissions have a strong non-LTE influence, similar to CO, but the retrieval of NO from MIPAS spectra has two additional problems: the nighttime concentration is small, preventing a nighttime-only, LTE retrieval; and there is a large, but poorly-determined, concentration at high-altitudes which significantly contributes to radiation from the nominal range of tangent paths.

Microwindows have been selected for LTE and non-LTE retrievals (i.e., jointly with vibrational temperature), as with CO, but here both cases are for a mid-latitude day-time atmosphere. Variations in the high altitude column are ignored, effectively assuming that the high altitude column is fixed. The selected microwindows are listed in Tables 31 and 32 and plotted in Figs. 62 and 63. For the LTE case the maximum of 10 microwindows was reached, while for the non-LTE case the maximum of 10 000 measurements was reached, the non-LTE microwindows being significantly wider than the LTE microwindows.

Table 31: NO LTE Microwindows

MW	Waveno. Range		Alt.		NPts	NUse
1	1860.375	1860.850	12	52	260	259
2	1874.825	1876.100	12	33	416	381
3	1887.450	1887.725	12	52	156	156
4	1923.350	1924.600	18	52	561	560
5	1850.050	1850.300	12	39	110	110
6	1928.625	1929.225	9	52	350	350
7	1857.225	1857.850	36	52	130	122
8	1931.525	1931.900	9	52	224	224
9	1830.275	1832.450	47	60	264	181
10	1870.000	1871.950	9	47	1027	434
				Total:	3498	2777

Table 32: Joint NO,T_{vib} (non-LTE) Microwindows

MW	Waveno. Range		Alt.		NPts	NUse
1	1847.650	1850.650	9	68	1936	1234
2	1873.775	1876.350	9	68	1664	1662
3	1852.250	1855.250	9	68	1936	1586
4	1855.575	1858.575	9	52	1694	1524
5	1844.625	1847.625	9	68	1936	1260
6	1897.650	1900.650	9	52	1694	1178
				Total:	10860	8444

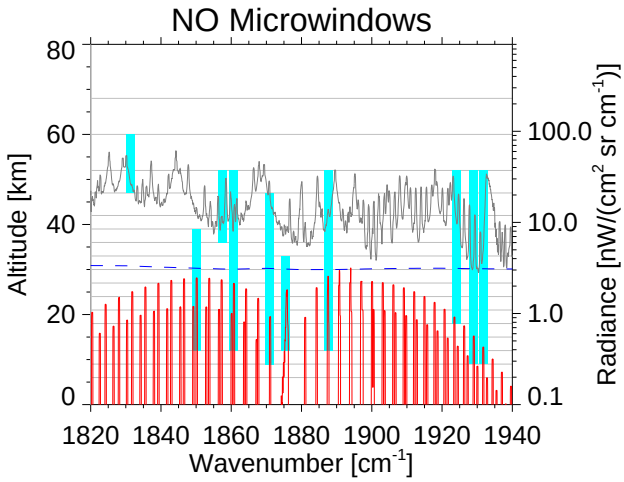

Figure 62: NO LTE microwindows and the NO spectrum.

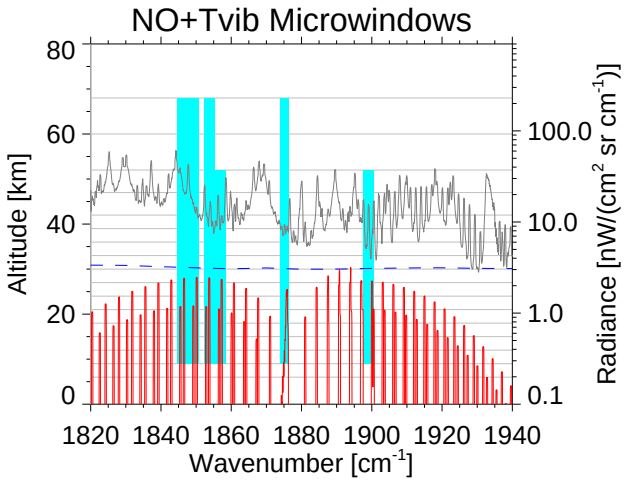

Figure 63: Joint NO,T_{vib} (non-LTE) microwindows and the NO spectrum.

Fig. 64 shows the NO profile and expected accuracy for the LTE case, and Fig. 65 the (kinetic−vibrational) temperature profile and expected accuracy for the non-LTE case. Results are summarised in Fig. 66.

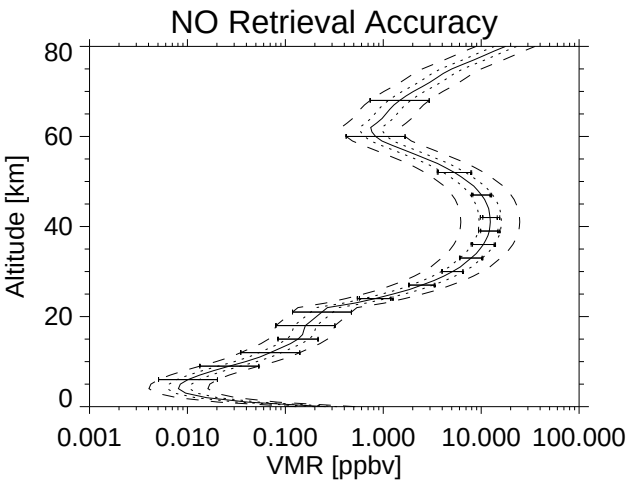

Figure 64: NO profile and retrieval errors for a mid-latitude day-time scenario assuming LTE. The dashed lines represent the ±100% *a priori* uncertainty and the dotted lines the ±30% limit of 'useful' accuracy. Inner ticks on error bars are precision, outer ticks are accuracy.

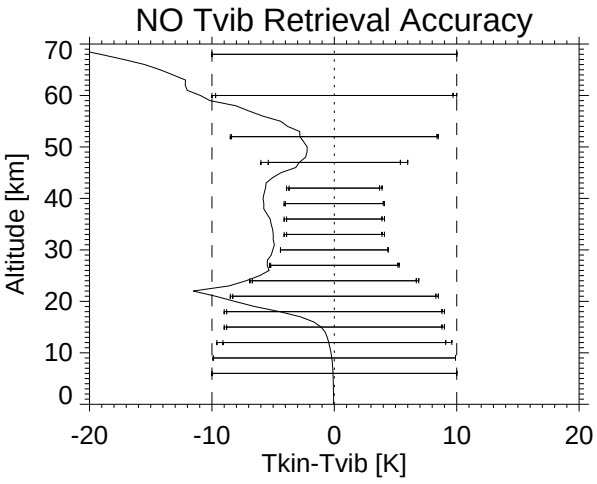

Figure 65: Difference between the kinetic and vibrational temperatures, and retrieval errors for mid-latitude day-time scenario assuming a joint NO,$T_{\rm vib}$ retrieval. The dashed lines represent the ±10 K *a priori* retrieval uncertainty.

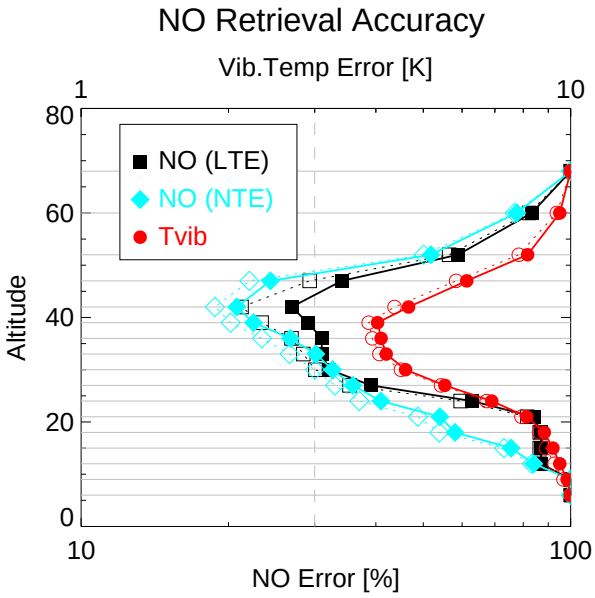

Figure 66: Retrieval accuracy profiles for NO assuming LTE, and for NO (NTE) jointly with $T_{\rm vib}$ (top axis), all in mid-latitude day-time conditions. Solid symbols/lines are accuracy, open symbols/dashed lines are precision.

Fig. 66 suggests that NO can be retrieved to useful accuracy in the altitude range 33–42 km, and that results are significantly improved at all altitudes if retrieved jointly with vibrational temperature. For an LTE retrieval precision is comparable with the non-LTE case but the accuracy is severely limited by non-LTE effects.

However, these represent optimistic cases. It is emphasised that the effects of the high altitude NO column and its uncertainty have not been considered in this analysis.

4.6.3 CO_2

In the operational processor, CO_2 emission features are used for the pT retrieval on the assumption that the CO_2 profile is fixed. In order to remove this assumption, microwindows have been selected for such a joint retrieval of CO_2, pressure and temperature, including the same *a priori* pointing information as used for the p, T retrieval. A related problem is that, since variations in CO_2 are generally small, a correspondingly more severe definition of 'useful' accuracy is required: $\pm 3\%$ (instead of $\pm 30\%$ used for other molecules).

Table 33: Joint CO_2, p, T Microwindows

MW	Waveno. Range		Alt.		NPts	NUse
1	685.200	688.200	6	68	2057	773
2	1931.750	1934.425	6	36	1188	548
3	1683.575	1684.800	6	30	450	274
4	739.325	742.325	47	68	484	334
5	696.325	696.775	6	52	285	284
6	713.800	714.475	15	39	252	252
7	688.225	688.650	6	52	270	261
8	1282.975	1283.925	6	24	273	157
9	1653.425	1654.425	6	30	369	254
10	1634.975	1635.375	6	30	153	119
				Total:	5781	3256

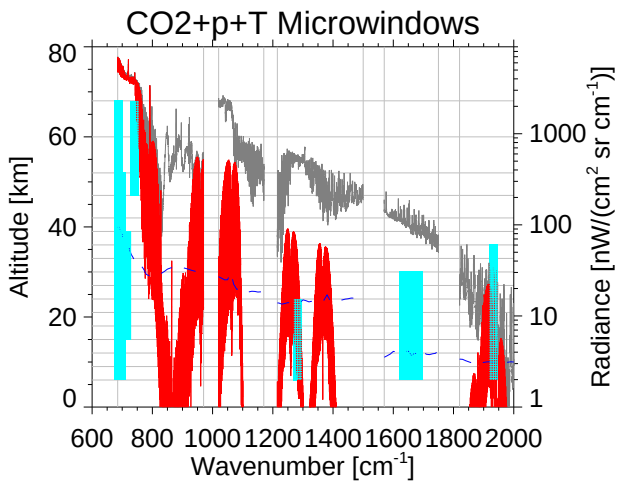

Figure 67: Joint CO_2, p, T microwindows and CO_2 spectrum.

Selected microwindows (limited to 10) are listed in Table 33 and plotted in Fig. 67. Note that several microwindows are selected in the relatively transparent 1650 cm^{-1} region which contains no CO2 lines. These may be using the O_2 continuum feature or weak CH_4 lines. Expected accuracy profiles for the retrieved parameters are shown in Figs. 68 and 69.

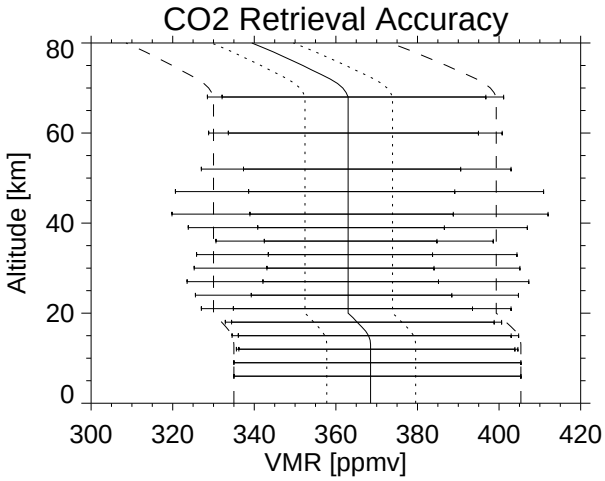

Figure 68: Assumed CO_2 profile and retrieval errors. Dashed lines indicate $\pm 10\%$ *a priori* uncertainty, dotted lines indicated $\pm 3\%$ 'useful' accuracy. Error bars indicate accuracy (outer marks) and precision (inner marks).

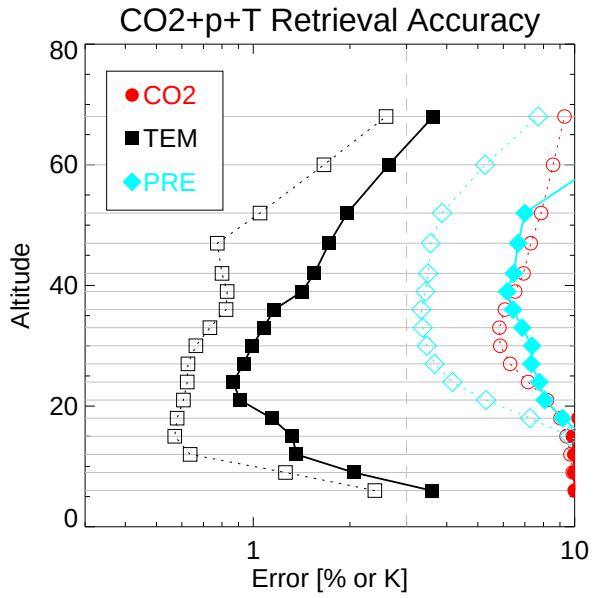

Figure 69: Retrieval errors for the joint CO_2, pressure and temperature microwindows. Solid symbols/lines are accuracy, open symbols/dashed lines are precision.

The results show that while temperature is retrieved with comparable accuracy to the current p, T retrieval (see, for example, Fig. 2), there are problems distinguishing CO_2 and pressure and neither is retrieved with useful accuracy. However, this includes a large ($\pm 25\%$) continuum uncertainty error. If the O_2 continuum in particular were better defined, this might provide independent pressure information at low altitudes.

References

[1] Atmospheric Infrared Sounder (AIRS),
http://www-airs.jpl.nasa.gov/

[2] Interferometric Monitor for Greenhouse Gases (IMG),
http://www.eorc.nasda.go.jp
/ADEOS/Project/Img.html

[3] Michelson Interferometer for Passive Atmospheric Sounding (MIPAS),
http://envisat.esa.int/instruments/mipas/

[4] Infrared Atmospheric Sounding Interferometer (IASI),
http://www-projet.cst.cnes.fr:8060/IASI/

[5] Tropospheric Emission Spectrometer (TES),
http://tes.jpl.nasa.gov/

[6] C. D. Rodgers,
Information content and optimisation of high spectral resolution measurements,
in *Optical Spectroscopic Techniques and Instrumentation for Atmospheric and Space Research II*, P. B. Hays and J. Wang (Eds.), Proc. SPIE **2830**, 136–147 (1996)

[7] C. D. Rodgers,
Information content and optimisation of high spectral resolution remote measurements,
Adv. Space Research **21**, 361–367 (1998).

[8] F. Rabier, N. Fourrié, D. Chafaï and P. Prunet,
Channel selection methods for infrared atmospheric sounding interferometer radiances,
Q. J. R. Meteorol. Soc. **128**, 1–15 (2001).

[9] T. von Clarmann and G. Echle,
Selection of optimized microwindows for atmospheric spectroscopy,
App. Optics **37**, 7661–7660 (1998).

[10] G. Echle, T. von Clarmann, A. Dudhia, J.-M. Flaud, B. Funke, N. Glatthor, B. J. Kerridge, M. López-Puertas, F. J. Martín-Torres and G. P. Stiller,
Optimized spectral microwindows for MIPAS-Envisat data analysis,
App. Optics **39**, 5531–5540 (2000).

[11] A. Dudhia. V. L. Jay and C. D. Rodgers,
Microwindow selection for high-spectral-resolution sounders,
App. Optics, **41**, 3665–3673 (2002).

[12] C. D. Rodgers,
Inverse Methods for Atmospheric Sounding: Theory and Practice
World Scientific Publishing Company (2000).

[13] N. Glatthor, T. von Clarmann, G. Echle, U. Grabowski, and E. Kimmich,
Optimized spectral microwindows for midlatitude and polar trace gas retrieval from MIPAS-ENVISAT measurements,
in *Remote Sensing of Clouds and the Atmosphere V*, J.E. Russell, K. Schfer, O. Lado-Bordowsky (Eds), Proc. SPIE **4168**, 343–353 (2001).

[14] Advanced MIPAS L2 Data Analysis (AMIL2DA), an EU Framwork V Project.
http://www-imk.fzk.de:8080/imk2/ame/amil2da/

[15] S. A. Clough, M. J. Iacono and J-L. Moncet,
Line-by-Line Calculations of Atmospheric Fluxes and Cooling Rates: Application to Water Vapour,
J. Geophys. Res. **97**, 15761–15785 (1992).

[16] D. P. Edwards,
GENLN2: A General Line-by-line Atmospheric Transmittance and Radiance Model. Version 3.0 Description and User's Guide,
Report *NCAR/TN-367+STR*, NCAR, Boulder, CO, USA (1992).

[17] L. L. Gordley, B. T. Marshall and D. A. Chu,
LINEPAK: algorithms for modeling spectral transmittance and radiance,
J. Quant. Spectrosc. Radiat. Transfer **52**, 563–580 (1994).

[18] A. Dudhia,
The Reference Forward Model (RFM)
http://www.atm.ox.ac.uk/RFM/

[19] B. T. Marshall, L. L. Gordley and D. A. Chu,
BANDPAK: algorithms for modeling broadband transmission and radiance.
J. Quant. Spectrosc. Radiat. Transfer **52**, 581–599 (1994).

[20] C. J. Marks and C. D. Rodgers,
A Retrieval Method for Atmospheric Composition From Limb Emission Measurements,
J. Geophys. Res. **98**, 14939–14953 (1993).

[21] L. M. McMillin, L. J. Crone and T. J. Kleespies,
Atmospheric transmittance of an absorbing gas. 5. Improvements to the OPTRAN approach,
App. Optics **34**, 8396–8399 (1995).

[22] R. Saunders, M. Matricardi and P. Brunel,
An improved fast radiative transfer model for assimilation of satellite radiance observations,
Q. J. R. Meteorol. Soc. **125**, 1407–1425 (1999).

[23] D. S. Turner,
Absorption coefficient estimation using a two-dimensional interpolation procedure,
J. Quant. Spectrosc. Radiat. Transfer, **53**, 633–677 (1995).

[24] L. L. Strow, H. E. Motteler, R. G. Benson, S. E. Hannon and S. de Souza-Machado,
Fast Computation of Monochromatic Infrared Atmospheric Transmittances using Compressed Look-Up Tables,
J. Quant. Spectrosc. Radiat. Transfer **59**, 481–493 (1998).

[25] M. Ridolfi, B. Carli, M. Carlotti, T. von Clarmann, B. M. Dinelli, A. Dudhia, J-M. Flaud, M. Höpfner, P. E. Morris, P. Raspollini, G. Stiller and R. J. Wells,
Optimized Forward Model and Retrieval Scheme for MIPAS Near-Real-Time Data Processing,
App. Optics **39**, 1323–1340 (2000).

[26] A. Dudhia, P. E. Morris and R. J. Wells,
Fast monochromatic radiative transfer calculations for limb sounding,
J. Quant. Spectrosc. Radiat. Transfer, **74** 745–756 (2002).

[27] J. Humlíček,
Optimized computation of the Voigt and complex probability functions,
J. Quant. Spectrosc. Radiat. Transfer **27**, 437–444 (1982).

[28] W. H. Press, B. P. Flannery, S. A. Teukolsky and W. T. Vetterling,
Numerical Recipes,
Cambridge University Press (1986).

[29] J-M. Flaud,
Review of Spectroscopic Parameters, WP1300 of ESA Contract 16700/02/I-LG, June 2003.